Controlling a doubly-fed induction machine for propulsion and charging of wireless powered rail transportation

Master Thesis

M.A. Postma

TU Delft

Controlling a doubly-fed induction machine for propulsion and charging of wireless powered rail transportation

Master Thesis

by

M.A. Postma

to obtain the degree of Master of Science at the Delft University of Technology, to be defended publicly on Monday October 25th, 2021 at 10:00 AM in TU Delft's Pulse Hall 4.

Student number:	4563638	
Project duration:	November, 2020 – October, 2021	
Thesis committee:	Prof. dr. ir. P. Bauer,	TU Delft, supervisor
	Dr. J. Dong,	TU Delft
	Ir. M. Cvetkovic,	TU Delft

An electronic version of this thesis is available at `http://repository.tudelft.nl/`.

TU Delft

Abstract

Traditional trains, with steel rails and wheels, have been around for centuries. The very good energy efficiency of steel-wheeled trains is one of the reasons that they are one of the more promising transportation modes in the future, where energy conservation becomes more and more important. Furthermore, electric trains are able to efficiently use sustainable power. They usually power their on-board motors by a sliding contact, with an overhead catenary wire or a 'third' power rail. However, trains using a linear motor have also emerged. These have several advantages: the amount of moving parts is reduced and the amount of traction force available is independent of the slipperiness of the tracks. Some systems still use a 'third rail' for power transfer however, which is a sensitive moving part and limits the train speed. Furthermore, arcs can cause damage under reduced air pressure. This may be eliminated using a linear doubly-fed induction machine (DFIM), which may be able to simultaneously propel and provide power to the train. The latter can be used to charge an on-board battery, which can provide the energy to keep the velocity constant between the stations, where active tracks may be omitted to save costs.

In this thesis, the use of a DFIM for a train application has been reviewed. A linear DFIM has been designed in a previous work [1], whose parameters are used in this thesis to simulate the concept. A controller is to be designed which allows the prescribed use of simultaneous propelling and charging. This thesis explores the requirements and possible controller candidates for the train application, which is followed by simulation and laboratory testing.

The application for a vehicle drive provides unique objectives and restrictions. One of the most restricting elements is that preferably no trackside (stator) quantities should be required for the control of the DFIM. After all, requiring trackside quantities would require a critical very dependable communication link between the track and vehicle. For this reason, estimation methods have been selected to control the vehicle with only vehicle-side measurements.

Three main categories of controllers have been identified: field-oriented control, direct torque control, and model predictive control. It has been found that each controller family has its advantages and disadvantages, and the best controller depends on the final system design of the train system. Field oriented controllers have the lowest current ripple, and can therefore be very predictable and efficient. Direct torque control is best used if it becomes very important to keep the final algorithm very simple. A model predictive controller excels if additional constraints are required, such as when using a multilevel inverter that requires balancing. This thesis provides a selection that can be used to make a decision in a later stage.

The operational principle of the train with the DFIM has been verified with a simplified laboratory test. A rotary DFIM has been powered with a fixed grid frequency-powered stator and an inverter-controlled rotor. Using a simplified control algorithm, the experiments have verified that the DFIM can be used to charge the vehicle at a high efficiency of up to 85%, and that the DFIM can indeed be used to simultaneously charge the vehicle and provide a tractive force. Additionally, a Simulink-simulation is performed where the performance of the linear DFIM design is validated. It has been concluded that the DFIM is an attractive candidate for use with a linear motor-driven train since it can indeed fulfil the roles of both motor and charger simultaneously and efficiently.

Preface

Writing this thesis was not always easy. It has sometimes been difficult to maintain an outlook when working on this thesis for the good part of a year. With the restrictions due to the coronavirus, it unfortunately has meant a lot of hours working at my desk in my 11-square meter student room. Fortunately, I received wonderful support to keep working and improving my thesis. Especially my girlfriend, Caroline, has always supported and trusted me, which helped immensely.

Special thanks goes out to Jianning Dong, who has been my daily supervisor during this thesis. Especially his trust in me was continuously encouraging me, without ever pushing. When I received a circuit board that seemed broken straight from the factory *twice*, I was convinced that I had made an error somewhere. But Dong immediately took them to check, and found out that it indeed was a design issue from the factory. Finally, Dong was always quick to answer my mails and give feedback, sometimes within hours. His help and trust were very useful during the development of this thesis.

Although there were ups and downs, I am now happy with the result. I am also very glad to have finished my Master's degree in Electrical Engineering at the University of Delft. The study program has given me broad knowledge about pretty much all subjects that the profession is rich, and this thesis gave me the chance to dive deeper into the world of electric drives. Even though studying was not always easy, electrical systems still enjoy me, and enjoy me even more now that I finally understand how they work. I'm very much looking forward to putting this knowledge in practice.

M.A. Postma
Delft, September 2021

Contents

1 Introduction 1

1.1 Description of the train system . . . 1

1.2 Objectives & methodology . . . 2

1.2.1 Research questions . . . 4

1.3 Report structure. . . . 4

2 Anticipated usage of the DFIM 5

2.1 Operation modes . . . 5

2.1.1 Slip of an induction motor . . . 5

2.1.2 Charging at standstill . . . 6

2.1.3 Acceleration . . . 6

2.1.4 Regenerative deceleration . . . 6

2.1.5 Single-fed operation . . . 7

2.2 Vehicle dynamics . . . 7

3 Modelling the doubly fed induction machine 9

3.1 Model identification . . . 9

3.2 Parameter identification of the rotary machine for laboratory testing . . . 10

3.2.1 Stator and rotor resistance measurement . . . 11

3.2.2 Open-circuit tests . . . 11

3.3 Model verification. . . . 12

3.3.1 Model verification results . . . 12

3.4 Machine model in the DQ-domain . . . 12

3.5 Universal model . . . 13

4 Control strategies for the DFIM 15

4.1 Vector control . . . 15

4.1.1 Estimation of the rotor field orientation . . . 17

4.2 Direct torque control . . . 18

4.3 Finite control set model predictive control . . . 20

4.4 Comparison between explored controllers . . . 22

5 Simulation on the application of the DFIM for the vactrain 23

5.1 Controller type for simulation and testing. . . . 23

5.1.1 Strategy 1: V/f control . . . 24

5.1.2 Strategy 2: Rotor resistance emulation . . . 24

5.2 Synchronous rectification with the linear DFIM. . . . 25

5.2.1 Synchronous rectification at standstill . . . 27

5.2.2 Synchronous rectification during acceleration . . . 27

6 Laboratory verification of the operation principles 31

6.1 Test setup . . . 31

6.1.1 DFIM Stator connection . . . 32

6.1.2 DFIM Rotor connection . . . 32

6.1.3 DC Machine . . . 32

6.2 Controller selection tests . . . 32

6.2.1 Laboratory testing the V/f controller . . . 32

6.2.2 Laboratory testing the rotor resistance emulator . . . 35

6.3 Performance measurements . . . 35

6.4 Conclusions from laboratory tests . . . 38

7 Discussion 39

7.1 Limitations of rotor resistor emulation . . . 39

7.1.1 Transient response . . . 39

7.1.2 Magnetic flux linkage control . . . 39

7.1.3 Lack of negative feedback . . . 40

7.2 Limitations of the vactrain simulation . . . 40

8 Conclusion 43

8.1 Applicability of a DFIM for simultaneously charging and propulsion . . . 43

8.2 Suitability of control algorithms. . . . 44

8.2.1 Resistance emulation . . . 44

8.2.2 Best suited controller types . . . 44

8.3 Final conclusion . . . 45

Bibliography 47

1 Introduction

For centuries, railways have used steel rails to guide trains in the open air. This has proven to have a number of advantages over other modes of transport: for example, trains have a very low rolling resistance, allowing heavy trains to achieve large speeds without much energy expenditure. It also allowed electric overhead lines to easily provide traction power. After the 1950s, many railways started building rail lines with increased speeds, regularly reaching 320 km/h, using the same conventional track structure [17]. The system of steel tracks has therefore been proven to provide a basis for even the most modern transportation.

In most recent times, pioneers are looking towards ways to increase train speeds even further than possible now. Furthermore, a key point of interest lays in the energy use of modern transport: to combat climate change, the energy use of transportation must be brought down. The search for this even faster and more efficient railway has lead to the origin for this thesis.

1.1. Description of the train system

To accelerate the development of rapid trains, recent research has suggested the use of linear propulsion motors, while upholding the use of traditional rails, since it provides the lowest possible energy use per passenger-kilometre [18]. To allow very high speeds, the ambient pressure is reduced, giving the system its name 'vacuum train' or vactrain. The vactrain uses a tube, or tunnel, in which the atmosphere is partly evacuated. This decreases the air resistance significantly compared to atmospheric pressure at sea level. A comparison of this system's energy usage with other transportation concepts can be seen in Figure 1.1.

Due to the very high speeds and the low dielectric strength of low-pressure air, a combination of overhead wire and pantograph will not be usable anymore, which is why a non-friction based power transfer method becomes necessary. A track-fed linear motor near stations would be an elegant solution, as it may be able to both charge the vehicle as well as provide a basis for rapid acceleration and deceleration. Outside of the stations, energy stored in on-board batteries is sufficient to maintain velocity, which eliminates the need for active track along long distances. This combination allows for relatively cheap track structures between the stations.

The researched candidate for the linear motor in this thesis is a linear doubly-fed induction motor (DFIM). With a DFIM, a propulsion force can be applied from both the track as well as the train, which are the stator and rotor in a traditional rotary machine. To provide trackside propulsion, electromagnets have to be built into the tracks along the entire length. This is referred to as active track. On the contrary, a passive track is not able to provide propulsion energy. In this case, the power to maintain speed has to come from the vehicles themselves. Urban railway systems using passive tracks are already widely used [13], but lack the capability to charge a vehicle.

To reduce costs, thereby making the system more economically promising, a system is proposed in [18] where

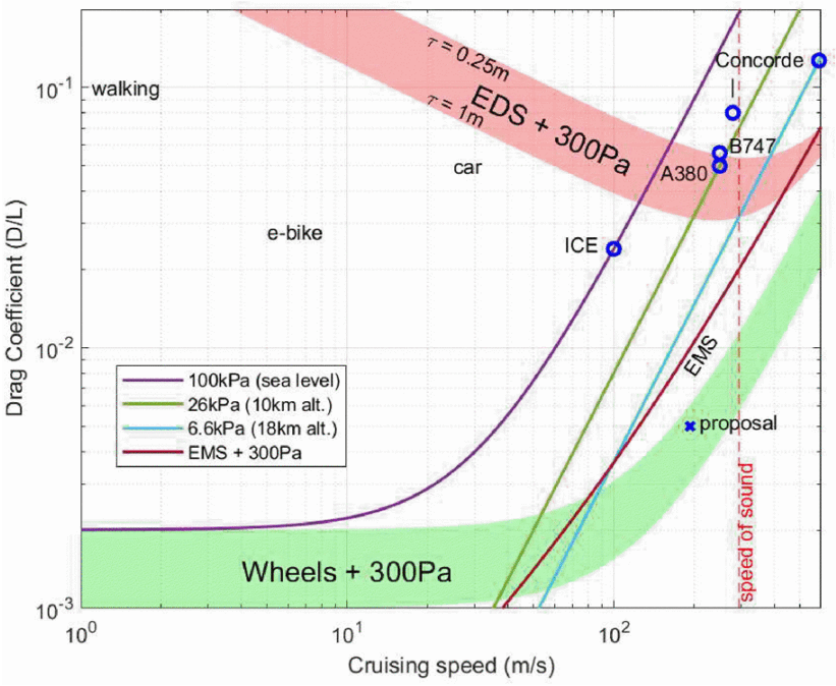

Figure 1.1: Drag coefficient comparison of track-based vactrain with other transportation modes [18]

passive tracks are used between terminals. This would not require expensive active tracks throughout the whole system. However, since the trains are now responsible to maintain speed between terminals, an energy storage system has to be built in to the vehicles themselves. This needs to be charged at the stations.

In this thesis, a system is presented where the vehicles are propelled and charged simultaneously within the terminals with the same DFIM. The double use of the machine allows to maximise the use of a single electromagnetic interface, which saves both the system's complexity as well as weight. Additionally, the vehicle-side part of the machine can be used in a passive track mode as well, reducing the active track length to a relatively small amount.

On the passive track sections, a number of different arrangements can be used. For example, the passive tracks can be arranged in a reluctance or induction fashion. Furthermore, a traditional rotary axle-driving machine can be used to drive the wheels, if this proves beneficial. A schematic overview of this vehicle concept is shown in Figure 1.2. This report will focus on the performance of the vehicle within the active track sections, where both propulsion and charging should occur simultaneously and where the vehicle operates as if it is driven by a doubly-fed induction machine.

1.2. Objectives & methodology

Various works have focused on the vactrain technology as described above. A high-level system design has been performed in [18], suggesting the use of the DFIM. Recently, a design study has been performed regarding the electromagnetic design of the DFIM [1]. This last work describes a machine design which has been conceptualised to be used with the vactrain system. However, a research into a suited controller lacks at the moment.

Like most vehicles, a train needs to have a form of speed control. Additionally, since the DFIM also doubles as a wireless charger, the power flow must be controlled as well. Such a double-function DFIM controller is not a traditionally researched subject. For this reason, the aim of this thesis is to explore suitable control algorithms, if possible, to use the structure of the doubly-fed induction machine to implement the required functionalities of propulsion and charging for a vactrain vehicle.

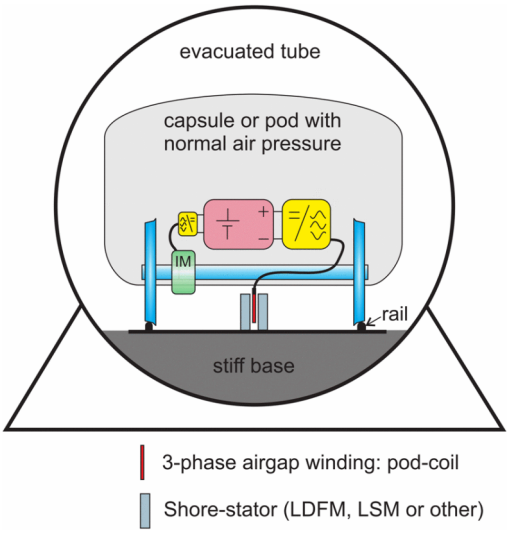

Figure 1.2: Vehicle concept consisting of both linear and rotary machines [18]

For this thesis, the electrical parameters as found in the design study of the DFIM [1] will be used for the final examination. For early testing purposes, and to allow physical concept validation, an available rotary machine will be described and used in the laboratory as well.

A linear doubly-fed induction machine capable of charging a vactrain vehicle has been designed in [1]. To be able to utilise this machine for the intended purposes, a controller needs to be developed. The controller is tasked with two main functions:

- Regulate the vehicle's acceleration and velocity.
- Regulate the power flow to and from the vehicle's battery. The amount of freedom to control this charging power independently of traction power is further described in Chapter 2.

These main functions may occur at the same time. To be able to manipulate the power flows, a power electronic converter is connected to the vehicle (rotor) side of the DFIM.

The objective of this thesis is to describe the process of the control system design for this doubly-fed induction machine. The available literature is researched to find existing control methods for (rotary) doubly-fed induction machines. These methods will be presented in this thesis, and a comparison will be made to aid the selection of the best candidate. A control algorithm will be made in Simulink, to simulate the behaviour of the controller with the machine. Furthermore, the concept will be tested by designing a basic controller for a TI Launchpad TMS320F28079D. This TI Launchpad creates a set of PWM waveforms which controls a three-phase full bridge PWM inverter, which is applied to the rotary DFIM. The behaviour of this laboratory setup will be verified against the requirements of the vactrain application.

A linear DFIM is by nature larger in size, and has less applications compared to the ubiquitous rotary electrical machines. Therefore, the TU Delft did not have a linear DFIM available, but they did have a rotary DFIM. This rotory DFIM is shown in Figure 1.3. Since the principles of operation remain the same, this machine is used to simulate the performance of the linear machine.

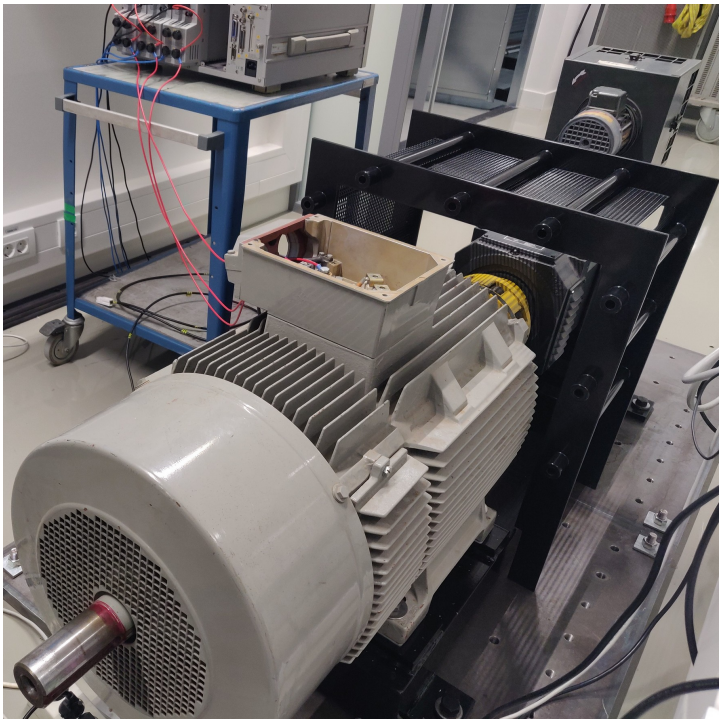

Figure 1.3: The available rotary doubly-fed induction machine, mechanically coupled to a DC machine

1.2.1. Research questions

How can a doubly-fed induction machine controller be designed to allow simultaneous propelling and charging a vactrain vehicle?

(a) To which extent is it possible to control the power flow to the batteries independent of the propulsion power?

(b) How can the machine be controlled to efficiently accelerate and decelerate the vehicle?

(c) Which type of controller is suitable for combining simultaneous propelling and charging the machine?

(d) How is it possible to omit a position sensor to effectively control the DFIM?

1.3. Report structure

The report is structured as follows:

- At first, the usage scenarios of the machine in the vactrain application will be described in more detail in Chapter 2.
- Then, the DFIM, which is the interface between the track and the vehicle, will be mathematically modelled in Chapter 3. This model will be used for simulation and control system design.
- Various possible control strategies which can control this model are explored in Chapter 4.
- A system simulation will be described in Chapter 5. This will provide a validation that the intended usage of the DFIM in the applied in a vactrain vehicle can function.
- Ultimately, the principles of operation can be validated in the laboratory setup as well. This is described in Chapter 6.
- Chapter 7 discusses the results: what has been achieved and what further work is needed?
- The conclusion of this thesis is presented in Chapter 8.

2

Anticipated usage of the DFIM

The doubly-fed induction machine is the main electric interface between the track and vehicle. It entails two main tasks: Propelling and braking the vehicle, as well as charging the vehicle's batteries. These functions provoke requirements for the control algorithms as explored in Chapter 4. In this chapter, the functions that the doubly-fed induction machine is to provide are described in more detail.

2.1. Operation modes

This section describes the foreseen usage of the final linear DFIM application in the vactrain vehicle.

For all operational modes, the tracks are foreseen to be shared between multiple vehicles at once. This condition may restrict later controller types: any controller that needs information about currents in the shoreside machine are not suitable, since the currents may not be flowing exclusively to that vehicle. Furthermore, if a controller depends on information of the stator, then propulsion will halt if the communication link falls away.

2.1.1. Slip of an induction motor

Under different operational conditions, different usage of the DFIM are foreseen. A DFIM can operate as an induction (asynchronous) machine [5]. This makes the slip of the machine an important parameter, since it defines the power flows of the machine. This subsection describes in short how the slip of the DFIM changes the operation conditions of the machine. Afterwards, the relation between operation of the vehicle (acceleration, deceleration, et cetera) will be linked with the power flow in the machine using the slip parameter.

First, a relation between the construction of the active track and the vehicle's speed is given. The layout of the track, together with the electrical frequency with which it is powered, determine a synchronous velocity v_0 of the trackside infrastructure. If the vehicles moves at this velocity, the magnetic field of the track and the vehicle are stationary relative to each other. Any difference in these velocities is the slip velocity. This corresponds with the slip frequency in a conventional induction machine. This slip can be calculated as:

$$s = \frac{\omega_0 - \omega}{\omega_0} = \frac{v_0 - v}{v_0} \tag{2.1}$$

Here, ω_0 references to the angular velocity of the synchronous speed of the machine, and ω refers to the rotor speed. With a linear machine, the variables can be expressed as a linear velocity.

If the slip is zero, the vehicle's velocity is stationary with respect to the magnetic field produced by the tracks. This means that no voltage can be induced into the vehicle's windings, and therefore no power transfer from

stator to rotor is possible.

The slip largely determines how the input power to the stator is shared between the mechanical output power and the rotor output (charging) power [5]:

$$P_m = P_s \cdot (1 - s) \tag{2.2a}$$

$$P_r = P_s \cdot s \tag{2.2b}$$

It is not desired that the vehicle spends energy from its battery on accelerating within the active track sections, since this would not use the availability of active track infrastructure optimally. For this reason, the synchronous velocity should lay higher than the achieved speed within the active track sections. This will make sure that the slip will stay positive, which will keep the outcome of Equation 2.2b positive. Additionally, this equation implies that the power to the rotor cannot be controlled independently from the mechanical output power. In all cases, the ratio of the velocity over the synchronous velocity determines how the power is shared between mechanical power and rotor power.

2.1.2. Charging at standstill

When the train is at standstill and within a station, it is foreseen to recharge its onboard batteries using the DFIM. This can occur while passengers have the opportunity to board and unboard. When standing still, the DFIM slip is:

$$s = \frac{v_0 - 0}{v_0} = 1 \tag{2.3}$$

During standstill, all the stator power will be able to charge the vehicle battery. One arising issue is that there is still torque developed. However, if the vehicle can be mechanically held in place by other means, the vehicle can still take charge without accelerating. To hold the vehicle stationary, a braking mechanism must therefore be applied. It is of great importance to prevent the vehicle from rolling or sliding away, as passengers may board or deboard the train during the charging process at standstill. For this reason, it would be best if the brakes hold the train passively. Additionally, wheel brakes may not always be reliable, especially in the case where the tracks are slippery. For these reasons, permanent magnet track brakes are foreseen to be used to brake the vehicle during standstill.

2.1.3. Acceleration

After the onboard batteries have been charged and the passengers (de)boarded, the vehicle should accelerate to depart at the station. As noted in section 2.1.1, the synchronous velocity is kept higher than the vehicle velocity, to allow for continuous charging of the battery. This means that the slip will always be positive:

$$0 < v < v_0 \implies 1 > s > 0 \tag{2.4}$$

During the acceleration phase, a constant stator power is foreseen. As follows from Equation 2.2, the mechanical output power will rise linearly with the vehicle velocity. This produces a constant traction force: $F = P_m / v$. Therefore, the vehicle accelerates with a constant acceleration. Meanwhile, the rotor power decreases with the same rate as the mechanical output power increases.

When the vehicle has not reached synchronous speed, the rotor power will always be positive when the vehicle is accelerating. Therefore, the battery must always be able to still take a charge when departing. Alternatively, in the case that the batteries can take less power than expected, resistors may be fitted to the vehicle to be able to continue acceleration. These resistors will also be needed when an electromagnetic braking action is needed quickly after leaving the station, with no other means to dissipate the power.

2.1.4. Regenerative deceleration

The vehicle spends the distance between the stations with a constant velocity. It is therefore foreseen that the vehicle will enter the station with about the same speed as with which it leaves. If the synchronous velocity of

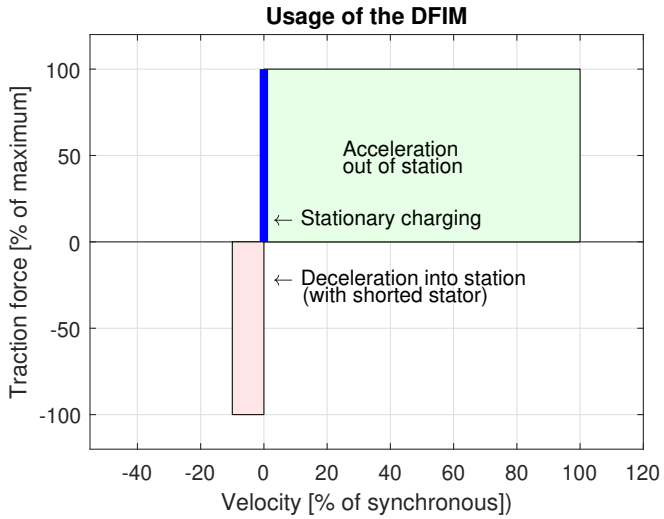

Figure 2.1: Foreseen usage of the DFIM

the trackside machine is not changed, the vehicle speed will again be below synchronous speed, and the slip s will be $0 < s < 1$. If the mechanical power is set to a negative value to slow the vehicle down, both the stator and rotor power change sign compared to acceleration as indicated in Equation 2.2. When decelerating during subsynchronous operation, the rotor power will therefore be negative. This implies that the battery of the vehicle is drained during braking, since power is transferred from rotor to stator. This is highly undesirable.

To prevent battery drain during deceleration, the stator windings under the vehicle may be shorted: a DFIM powered from the rotor side with a shorted stator is comparable to a traditional induction machine [16], but with the roles of stator and rotor reversed. This will make the rotor slip negative. With a negative slip, a negative mechanical power results in a positive rotor power. This allows the vehicle to regenerate the braking energy back into the vehicle's battery. Trackside stator-shorting switchgear adds relatively little complexity to the stator system.

A graphical representation of the operation modes of the DFIM is given in Figure 2.1. It shows that the DFIM slip is positive while accelerating. When decelerating, it is negative and relatively low.

2.1.5. Single-fed operation

Outside of the stations, passive tracks are foreseen. Although the passive track sections are not the focus in this study, a number of arrangements are foreseen. Passive tracks can be arranged in a reluctance, induction or permanent magnet fashion. Furthermore, a traditional rotary axle-driving machine can be used to drive the wheels, since the high-power acceleration and power transfer capability are not required during cruising. This would allow the passive track structure to omit a stator arrangement in the track sections where no active track is provided.

During normal operation, the vehicle only has to be able to maintain its speed. However, in cases of emergency, the vehicle should also always be able to decelerate rapidly, and accelerate again afterwards. In the case of re-acceleration, the efficiency and speed is allowed to be lower since it only occurs during nonstandard operation.

2.2. Vehicle dynamics

In this section, the vehicle dynamics are described. This model is used to simulate the behaviour of the complete system, which will later be described in Chapter 5. A simple model of the vehicle, consisting of the propulsion forces, the friction and the inertia, is used. Such a model is sufficient for simulating the vehicle

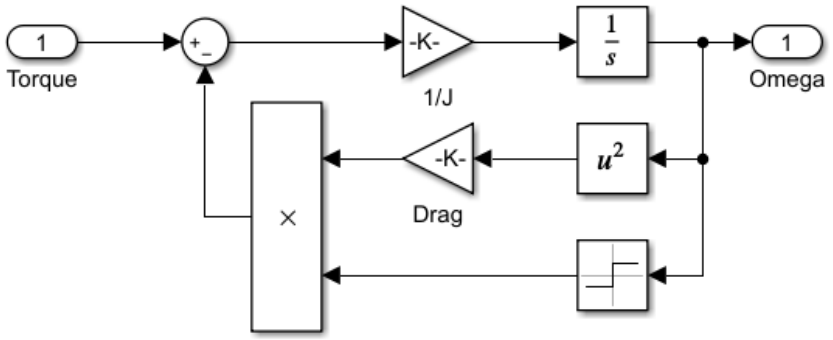

Figure 2.2: Simulink model of mechanical subsystem

Item	Value	Unit
Mass	10 000	kg
Cruise speed	700	km/h
DFIM power	1000	kW
Cruising drag force	400	N
Air density	300	Pa
$c_w A_{front}$	3	m^2

Table 2.1: Vehicle unit specifications [18]

velocity and therefore the influence of the acceleration and velocity on the vehicle and DFIM.

The vehicle is represented as a mass, on which can the force of the linear induction motor as well as the frictional forces are exerted. The vehicle accelerates according to Newton's law:

$$v = \int a\,\mathrm{d}t + v_0 = \int \frac{F}{m}\,\mathrm{d}t + v_0 \tag{2.5}$$

The force F consists of the motor force F_m and the frictional force F_w:

$$F = F_m + F_w \tag{2.6}$$

Finally, this frictional force consists of a constant 'dry' friction F_{wc} as well as a velocity-dependent friction F_{wv}:

$$F_w = -\operatorname{sign} v\big(F_{wc} + \underbrace{c_{wv}\cdot|v|^2}_{F_{wv}}\big) \tag{2.7}$$

The dry friction, representing the wheel-rail friction and other rolling resistances, approximates to 200 N. The air resistance force of the vehicle depends, except for the speed squared, on the air density ρ, the frontal area of the vehicle A_{front}, and the air resistance coefficient c_w. For the vehicle, this equates to [18]:

$$c_{wv} = \frac{1}{2}\rho A_{front} c_w = \frac{1}{2}\cdot 0.0035 \cdot 3 = 0.0053\ \mathrm{N/(m/s)^2} \tag{2.8}$$

The individual quantities are listed in Table 2.1. A Simulink-model of this mechanical subsystem has been made and is shown in Figure 2.2.

In Table 2.1, the specifications of a singular vehicle unit are listed. The specifications are required for simulations of the complete vehicle. These specifications are based on earlier work [18]. It is noted that a train may be composed of multiple vehicle units. The formation of a train can allow lower air resistance, by decreasing the frontal area of the vehicle per passenger. Furthermore, tightly coupled vehicles allow for a larger passenger throughput. Finally, by sharing components, weight may be saved as well. Although the vehicles are foreseen to be coupleable, all simulations on the vehicle are done with a singular vehicle unit. This way, the worst-case scenario regarding the air resistance is considered.

3

Modelling the doubly fed induction machine

This chapter describes the construction of a (doubly fed) induction machine model, as far as relevant for its control. This model is later used to develop the control system and simulate the expected behaviour before it is implemented on hardware.

The stationary part of an electrical machine is named the stator, while while the rotating part is the rotor. These terms are used within this chapter for a linear machine as well; in that case the rotor is considered to be the vehicle. An induction motor has windings on both the stator and rotor.

In a doubly-fed induction machine, the rotor winding terminals are available so an external voltage can be applied to it. On a rotating machine, a voltage can for example be applied via carbon brushes on sliprings. In this study, where a linear machine is to be applied for a train that partly rides on passive track, the rotor currents are be controlled on the rotor side (on-board) using stored battery power. The rotating test setup in the laboratory has its rotor currents applied using slip rings.

Some assumptions are made to keep the model mostly linear:

- The machine's air gap is constant, so that the magnetic reluctance is equal in the d and q directions.
- The magnetic materials are linear; so no saturation occurs.
- Magnetic hysteresis, eddy currents and skin effect are ignored.
- The windings are sinusoidally distributed, so a balanced set of currents create a uniformly rotating magnetic field.

3.1. Model identification

In order to predict the machine behaviour and later design a controller, a machine model is required. Various models exist with varying degrees of accurateness: Models can in- or exclude saturation or skin effects. In the simplest form, the machine can be modelled as having a set of coupled coils on the stator and rotor. With stator coils L_s and rotor coils L_r coupling factor can be defined as:

$$k = \frac{M}{\sqrt{L_s \cdot L_r}} \tag{3.1}$$

For a rotary machine, this coupling factor k is expected to be more than 0.9.

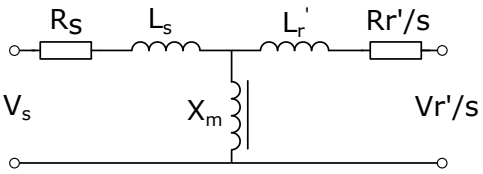

Figure 3.1: Per-phase steady state machine model

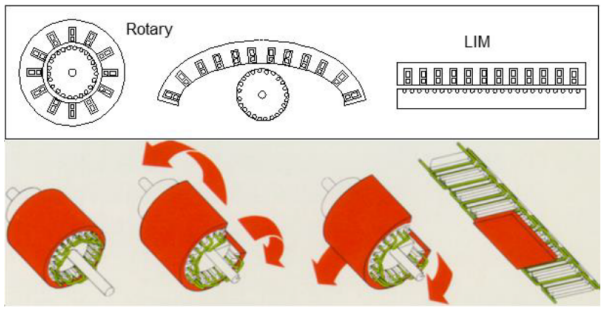

Figure 3.2: Unrolling a rotary machine into a linear machine [13].

The stator inductance can now be split into two parts: the magnetisation inductance L_m, with the rest of the inductance defined as leakage inductance $L_{\sigma s}$:

$$L_m = L_s \cdot k \tag{3.2a}$$

$$L_{\sigma s} = L_s \cdot (1-k) \tag{3.2b}$$

This can also be done with the rotor leakage inductance:

$$L_{\sigma r} = L_r \cdot (1-k) \tag{3.3}$$

With these paramaters, a T-circuit representation of the coupled coils can be made. In this representation, the turns ratio is eliminated and either the circuit is drawn as stator or the rotor terminal impedance equivalent. Here, a stator reference is chosen. This way, the stator magnetisation inductance is used, and the rotor leakage inductance is transferred to the stator side:

$$L'_{\sigma r} = a^2 L_{\sigma r} \tag{3.4}$$

Where a, the machine's turns ratio, is calculated as:

$$a = \sqrt{\frac{kL_s}{kL_r}} = \sqrt{\frac{L_s}{L_r}} \tag{3.5}$$

Finally, the DC resistances are added to both windings. The rotor resistance is also referred to the stator side. The final per phase T-representation of the machine is shown in Figure 3.1.

3.2. Parameter identification of the rotary machine for laboratory testing

For early testing and simulation purposes, conceptual validation testing will be performed in the laboratory, as will be described in Chapter 6. No linear machine was available for laboratory testing, due to the relative uncommonness and bulkiness of linear machines. Therefore, these tests will be performed with a rotary DFIM.

A linear DFIM can be viewed as a 'rolled-out' rotary machine [13], as is demonstrated in Figure 3.2. Since rotary machines share the exact same principle of operation, this rotary machine can be used for early laboratory testing. In later simulations of the complete vehicle concept, the same model will be used, albeit with different parameters representing the linear machine.

A picture of the rotary machine is included in Figure 1.3. The nameplate data of the rotary machine in the laboratory is given in Table 3.1.

Parameter	Value	Unit
Stator line voltage	380	V
Stator phase current	51	A
Stator cosinus phi	0.74	-
Maximum duty cycle	100%	-
Nominal speed	970	RPM
Machine power	22	kW
Rotor line voltage	295	V
Rotor phase current	46	A

Table 3.1: Nominal nameplate data of the rotary doubly fed induction machine

3.2.1. Stator and rotor resistance measurement

With the machine unpowered and at standstill, the DC resistances of both the stator and rotor of the DFIM can easily be measured. A measurement is done where:

1. A DC current of around 5.0 A is injected into the stator or rotor winding. The exact current is measured using an accurate current meter.
2. The DC voltage across the motor terminals is measured. Here, the slipring brushes are included in the circuit, since they also are included in the final application.
3. The resistance is found as $R = V / I$

3.2.2. Open-circuit tests

After the stator and rotor resistances are known, the other parameters are found by measuring the line frequency impedances of both the rotor and stator, as well as the induced voltage in the unpowered winding:

1. With the rotor at standstill, the stator windings are powered. Using a three-phase autotransformer, the terminal voltage is increased until the per-phase current is about 5A. This current mimicks the magnetisation current to be used with the inverter. It is much less (<20%) than the saturation current.
2. The open-circuit voltage of a rotor winding is recorded.
3. The rotor is now powered, with the stator open circuit. The current is recorded, to calculate the rotor reactance from.

Unfortunately, test with the rotor and stator windings in series was not possible, since the internal star points are unreachable. When powering the stator and rotor windings, all three phases are connected to induce a rotating magnetic field into the receiving coil, so that the electrical characteristics are largely independent of the rotor position.

The following equations follow from the measurements:

$$X_s = X_m + X_{\sigma s} = \Im\left(\frac{V_s}{I_s}\right) \tag{3.6a}$$

$$X_r = X_m \cdot a^2 + X_{\sigma r} = \Im\left(\frac{V_r}{I_r}\right) \tag{3.6b}$$

$$|V_{ind,r}| = |I_s| \cdot X_m \cdot \frac{1}{a} \tag{3.6c}$$

$$a = \sqrt{\frac{X_s}{X_r}} \tag{3.6d}$$

Here, a is the turns ratio between the stator and rotor windings. With the measured values, the equations can be solved to find the machine reactances. To find the inductances, the reactances are divided by $2\pi \cdot 50$ (line frequency). The resulting machine parameters are listed in Table 3.2.

Parameter	Value	Unit
R_s	94	mΩ
R_r	105	mΩ
L_m	24.91	mH
$L_{\sigma s}$	0.95	mH
$L_{\sigma r}$	0.63	mH

Table 3.2: Per-phase machine parameters of the rotary DFIM

	Measurement		Modelled	
RPM	V_s (V)	$\cos\phi$	V_s (V)	$\cos\phi$
500	12.28	0.435	10.58	0.5325
950	41.79	0.832	44.71	0.8617
1050	34.96	-0.822	42.30	-0.8440
1405	11.69	-0.263	9.81	-0.3878

Table 3.3: Rotary DFIM model verification comparison

3.3. Model verification

To verify the machine model and its parameters, a comparison is made between the machine's real behaviour and the simulation. A set of machine measurements is done at grid frequency. The 22 kW machine was too large to start direct on line so the machine is connected to the mains voltage via a variable autotransformer. The rotor is shorted, creating a regular induction machine. The machine's rotational speed is set using an externally coupled DC motor. To stay within the current limits of the transformer, the applied motor voltage is raised until the current becomes 15 A.

Four rotational speeds are used: One near the nominal speed of 970 rpm, and one at a larger slip. The machine is used as motor and as generator alternately. At all of these rotational speeds, the terminal voltage and power factor are logged using a power analyser, to be able to compare it with the modelled machine.

These expected terminal voltage is also retrieved from the steady-state induction machine model with the calculated parameters. First, the total modelled machine impedance is calculated, and this is then multiplied by the current of 15A to find the expected terminal voltage of the machine:

$$Z = R_s + jX_{\sigma s} + \frac{jX_m \cdot (jX'_{\sigma r} + R'_r/s)}{jX_m + (jX'_{\sigma r} + R'_r/s)} \tag{3.7a}$$

$$V = 15Z \tag{3.7b}$$

3.3.1. Model verification results

The data from the simulation as well as the lab test are listed in Table 3.3 and plotted in Figure 3.3. It can be seen that the simulated values and the measured values are in the same order of magnitude, but that an error exists: all voltages seem to be a little more inductive than simulated. This might for example be because the leakage inductances are underestimated a bit. Further tuning of the machine parameters may later be done if the error is to be reduced.

3.4. Machine model in the DQ-domain

In section 3.1, the machine model is presented as the stator-equivalent circuit model. However, it can be advantageous to model the machine in a different domain, aligned to a pre-determined axis. This is especially useful with vector-oriented control, as discussed in Chapter 4. For this reason, a general transformation to the dq-domain is described in this section.

With the dq-frame aligned to the magnetic field, the voltage equations of induction machine windings in the

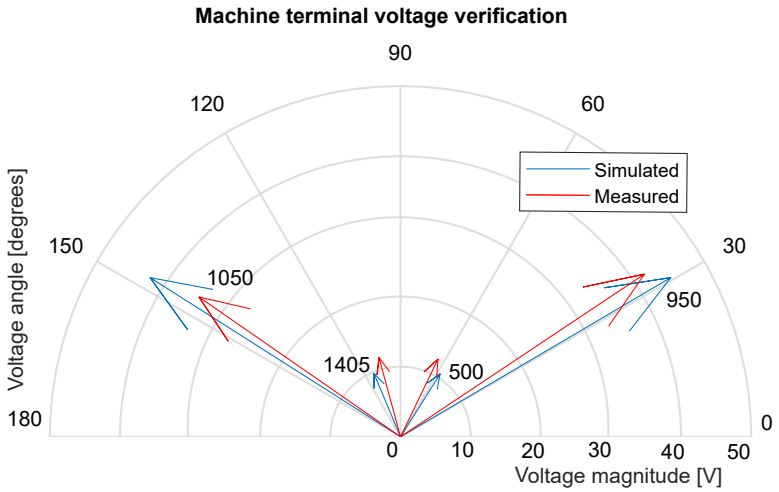

Figure 3.3: Comparison of measured and simulated terminal voltage at 15A phase current at different RPMs

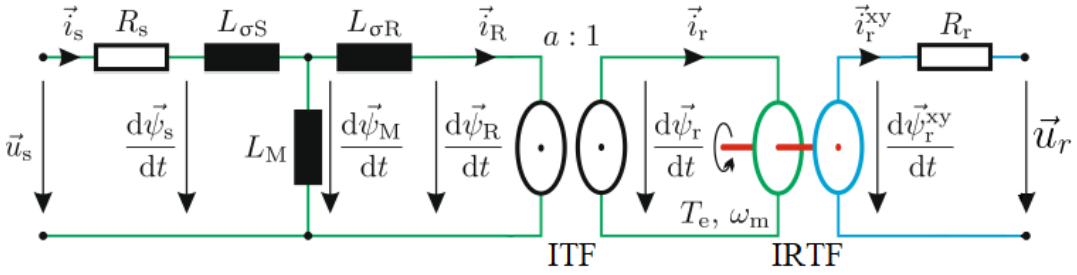

Figure 3.4: Universal model schematic of a doubly fed induction machine [4]

dq-reference frame are [4]:

$$\vec{u}_s^{dq} = R_s \vec{i}_s^{dq} + j\omega_s \vec{\Psi}_s^{dq} + \frac{\mathrm{d}}{\mathrm{d}t}\vec{\Psi}_s^{dq} \tag{3.8a}$$

$$\vec{u}_R^{dq} = R_R \vec{i}_R^{dq} - j(\omega_s - \omega_m)\vec{\Psi}_s^{dq} - \frac{\mathrm{d}}{\mathrm{d}t}\vec{\Psi}_R^{dq} \tag{3.8b}$$

Here, Ψ_s is the stator flux linkage. If the rotor voltage $\vec{u}_R^{dq} = 0$ in Equation 3.8b, the machine behaves as a conventional induction machine with shorted rotor windings.

The torque of the doubly-fed induction machine can be expressed as:

$$T = \frac{3}{2} p \vec{\Psi}^{dq} \times \vec{i}^{dq} \tag{3.9}$$

Both stator and rotor quantities can be used in Equation 3.9.

3.5. Universal model

By changing the virtual turns ratio, the parameters of the machine can be changed while keeping the impedance as seen from the DFIM terminals the same. This can be used to eliminate the stator- or rotor leakage inductance, which simplifies the model and control of the machine. The flux linkage of the machine can be written as:

$$\vec{\Psi}_s = L_s \vec{i}_s - L_m \vec{i}_r - aL_m \vec{i}_s + aL_m \vec{i}_s \tag{3.10}$$

With $L_s = L_m + L_{\sigma s}$ and $\vec{i_r} = a\vec{i_R}$, this can be rewritten as:

$$\vec{\Psi}_s = \underbrace{\left(L_s + aL_m\right)}_{L_{\sigma S}} \vec{i}_s + \underbrace{aL_m}_{L_M} \left(\vec{i}_s - \vec{i}_R\right) \tag{3.11}$$

A similar equation can be expressed for the rotor field:

$$\vec{\Psi}_R = aL_m \vec{i}_s - a^2 L_r \vec{i}_R - aL_m \vec{i}_R + aL_m \vec{i}_R \tag{3.12}$$

This can be written as:

$$\vec{\Psi}_R = \underbrace{aL_m}_{L_M} \left(\vec{i}_s - \vec{i}_R\right) - \underbrace{a^2 L_r - aL_m}_{L_{\sigma R}} \vec{i}_R \tag{3.13}$$

Here is used that $L_r = L_m + L_{\sigma r}$ and $\vec{\Psi}_R = a\vec{\Psi}_r$. This results in the following expression for the flux linkages of the stator and rotor. Summarised, the newly constructed inductances can be calculated as:

$$L_M = aL_m \tag{3.14a}$$

$$L_{\sigma S} = L_m\left(\frac{L_s}{L_m} - a\right) \tag{3.14b}$$

$$L_{\sigma R} = aL_r\left(a - \frac{L_m}{L_s}\right) \tag{3.14c}$$

The flux linkages can now be calculated as:

$$\begin{bmatrix} \vec{\Psi}_s \\ \vec{\Psi}_R \end{bmatrix} = \begin{bmatrix} L_M + L_{\sigma S} & -L_M \\ L_M & -L_M - L_{\sigma R} \end{bmatrix} \begin{bmatrix} \vec{i}_s \\ \vec{i}_R \end{bmatrix} \tag{3.15}$$

Finally, to transform the rotor resistance to the universal model parameter as well, it must be transformed to the stator side:

$$R_R = a^2 R_r \tag{3.16}$$

If a is chosen to be $a = \frac{L_m}{L_m + L_{\sigma r}}$, it can be seen that $L_{\sigma R}$ becomes equal to zero and is eliminated. This may simplify later analysis.

4

Control strategies for the DFIM

In this chapter, different candidates for the doubly-fed induction machine are explored, which are sufficiently advanced to be used as a final drive in a vactrain application. Three different approaches are selected: vector oriented control, direct torque control, and model predictive control. The main operating principles will be described in the following sections. The chapter is concluded with a comparison of the different candidates, with a preliminary selection of the most applicable candidate.

4.1. Vector control

In a vector controller, the controlled variables are stationary in a pre-determined reference frame. Values are measured in one domain, such as the stationary $\alpha\beta$ frame, and are transformed to the dq frame where the d or q axis is oriented along a pre-determined axis. Since these dq-domain variables are not fluctuating with the electrical frequency, they can be controlled with simple controllers such as PI-controllers. An orientation axis may be:

- Field-oriented control, often used in electric drives where torque and the field are decoupled. This field can be the stator, air gap or rotor field. [4]
- Stator-voltage oriented control, often used in power generation applications where active and reactive power can be readily controlled [8]. An overview of such a PQ-controller is given in Figure 4.1. In contrast to power generation applications, it is undesired to control stator quantities in the train application, since the active tracks can be shared between multiple vehicles.

To transform the stator values to the control reference frame, a Park transformation is used. The required angle may be directly determined by measurements (sensored operation), as well as indirectly by a model (sensorless operation).

The output from the controllers is a voltage, which is applied to a space vector PWM modulator. The general process of a vector oriented controller is:

1. The relevant quantities are measured using sensors. These include at least the rotor current.
2. Using a model of the DFIM:
   (a) The actual electromagnetic torque and magnetic flux linkage are estimated.
   (b) The reference dq-currents are calculated, to meet the reference torque and flux linkage.
   (c) If not measured using sensors, the magnetic field orientation is estimated. Section 4.1.1 describes some estimation methods.

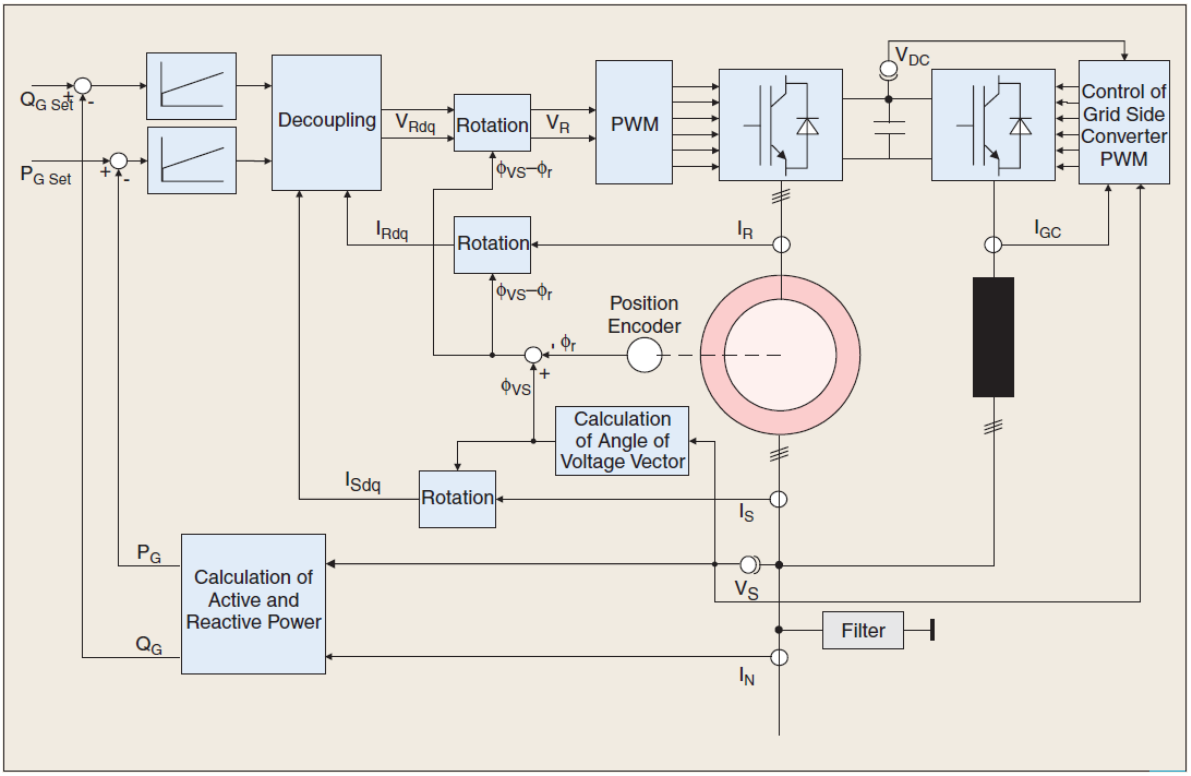

Figure 4.1: Vector PQ-control of a DFIM for wind energy generation [8]

3. The rotor current is transformed into the rotating reference frame (dq-frame) using the Clarke and Park transformations.

4. A set of current controllers compare the actual currents to the reference, and generate a dq-voltage reference. A decoupling network is used to cancel interference between the two controllers.

5. The dq-voltage from the controllers are transformed back into the stationary reference frame using the inverse Clarke and Park transformations.

6. A space vector modulator takes the desired output voltage and converts it to PWM duty cycles which are applied to the inverter.

The PI current controllers can be tuned analytically, by using the analytic model of the dq-referenced DFIM as presented in Chapter 3. A decoupling network is required to decouple both current controllers from each other. Then, the rest of the circuit can be simplified as an RL-circuit.

A speed controller may be used to generate a torque reference. This speed controller must be tuned to a bandwidth that is low compared to the current controller [4]. The difference in control bandwidths allow the control to be relatively decoupled. Since the target application in this thesis is a vehicle, which cannot rapidly adjust speed anyway, a relatively low speed controller bandwidth is not problematic.

The space vector modulator produces a constant frequency three-phase pulse width modulated output. Therefore, the frequency content of the current is very predictable and in a specific frequency band. This may prove beneficial if the current must be filtered at the shore-side.

A vector-oriented controller is often dependent on the reverse machine model to generate reference currents, especially when position and stator sensors are removed. The performance of the controller may degrade when the machine parameters are not known precisely. The PI-tuning, the PI decoupling network and possibly the field orientation all depend on the machine parameters. This can be a disadvantage of the vector control.

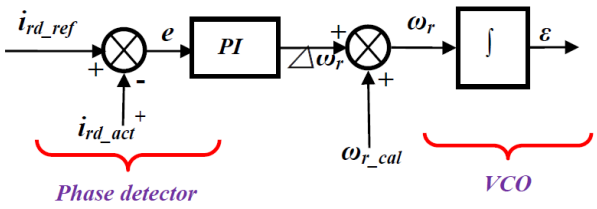

Figure 4.2: Rotor positioning scheme using rotor side PLL [9]

An extra constraint comes from the desire to have no stator current or voltage sensors. Requiring trackside sensors would imply that there needs to be a dependable and low-lag data link between the vehicle and the trackside for the vehicle not to behave erratic. This may cause undesired behaviour should the communication link be lost, and adds extra maintenance. Furthermore, a current sensor requirement would also rule out that an active track section can be used simultaneously by multiple vehicles. Therefore, such a requirement would be very restricting.

4.1.1. Estimation of the rotor field orientation

For vector-controlled operation, an orientation axis is required, which needs to be synchronous with the slip frequency in case of a DFIM. In a traditional squirrel-cage induction machine, the induced voltage and current in the rotor are equal to the slip frequency sf_s. Since the rotor mechanically rotates with speed $(1-s)f_s$, the frequency of magnetic field in the stationary reference frame is always f_s. The frequency of the magnetic field as seen by the stator is therefore always equal to the supplied grid frequency. In a doubly-fed induction machine, this condition is not automatically guaranteed: the rotor inverter may supply a voltage with a frequency that is unequal to the slip frequency. If the voltage applied to the rotor has a slightly different frequency compared to the slip frequency, than the rotor current will be modulated by the difference frequency, causing serious torque fluctuations. Therefore, the applied rotor voltage must have exactly the slip frequency, and indirect field estimators are ruled out [19].

Another point of view can be that a doubly-fed induction machine can be seen as a hybrid between a traditional induction machine and a synchronous machine [5]. If a synchronous machine is connected to the grid, the rotor velocity must be adjusted to the grid frequency. If this condition is not met, the torque developed will be very erratic. With a DFIM, a similar condition must hold: it can be satisfied by changing the rotor voltage frequency as well as the mechanical rotor velocity.

Since the applied rotor voltage frequency must always have the exact slip frequency, indirect field orientation structures such as a slip frequency estimator are unsuitable. Instead, a sensored or a direct field orientated approach must be used. However, a sensored approach is undesired in this application due to the extra required interface between vehicle and track. Adhering these constraints, two estimation methods have been identified, based on the rotor side induced voltage and a phase-locked loop which locks on the magnetisation current controller:

- **Rotor side induced voltage measurement**
  The rotor field angle can directly be retrieved from induced voltage [19]. This uses the same basic principle as in the direct torque controller, which is condensed in Equation 4.1. An extra set of measurement windings can also be used, to prevent measurement error due to rotor resistance deviations. However, a minimum slip frequency is always required for the induced voltage to be reliably detectable. That implies that the vehicle can never cross the synchronous velocity. Therefore, the synchronous velocity must be set higher than the maximum speed of the vehicle.

- **Rotor side phase locked loop**
  The rotor positioning can be made more reliable using a phase-locked loop (PLL). An elegant way of positioning using a PLL is presented in [9]. The presented PLL uses the magnetisation current controller of an existing vector controller to detect the rotor position. A schematic of this estimator is shown in Figure 4.2.

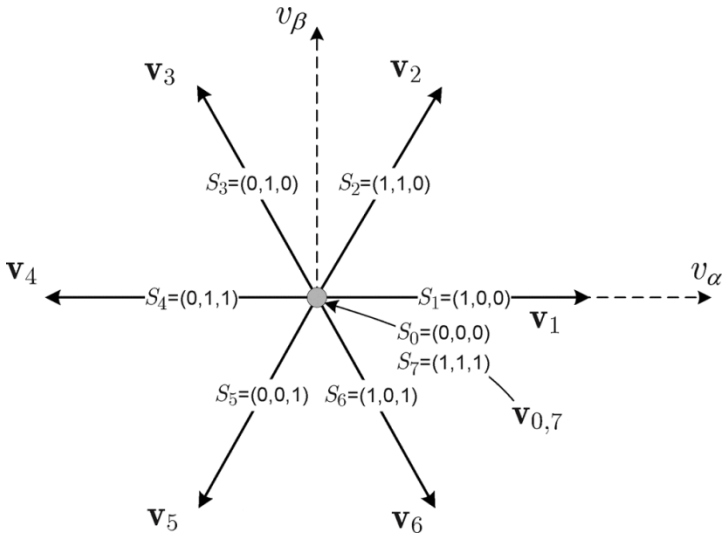

Figure 4.3: Possible switching states of a two-level voltage source inverter [6]

A large advantage of this method is that the PLL can be tuned to a bandwidth, in this case 100 Hz. This makes the estimation more robust: a short measurement error will not immediately throw the estimation off. Furthermore, the PLL is independent of the induced voltage, and can therefore be operated at synchronous velocity. This allows the stator frequency to be set slightly lower, which has the advantage of reducing the effect of the leakage inductances. The largest disadvantage is that the magnetisation current PLL can only be used with a rotor current controller. This excludes direct torque control and model predictive control.

- **High-frequency signal injection**
  A high-frequency voltage signal can be modulated on the trackside stator voltage, which can be read on the the vehicle side to infer the orientation of the magnetic field [15]. This method can also be used at synchronous velocity. The main disadvantage is the requirement for an extra trackside current injector. Additionally, such an estimator cannot seamlessly switch to single-fed operation outside of the active track area.

4.2. Direct torque control

With direct torque control, the voltage of either the stator or rotor (in a DFIM) in $\alpha\beta$-frame is used along with the stator or rotor resistance and currents to derive the flux linkage [12]:

$$\vec{\Psi}_s = \int \vec{u}_s - R_s \vec{i}_s \, \mathrm{d}t \tag{4.1}$$

Here, it is assumed that the stator is controlled. The flux linkage can be expressed in the magnitude as well as the angle. The magnitude is to be controlled to be within a pre-specified hysteresis band, representing the magnetic design values of the machine. Furthermore, the torque is also controlled by another hysteresis controller to be withing a band around the reference torque. The machine torque is estimated from the flux linkage and current:

$$\hat{T} = p\left(\hat{\Psi}_\alpha i_\beta - \hat{\Psi}_\beta i_\alpha\right) \tag{4.2}$$

The voltage-source inverter connected to the rotor terminals only have eight possible output states. Every state corresponds to a voltage vector, which can be used to steer the torque and magnetic flux towards a certain direction. A graphical representation of these voltage vectors is given in Figure 4.3. This is used to build a switching table which sets the voltage-source inverter's state based on:

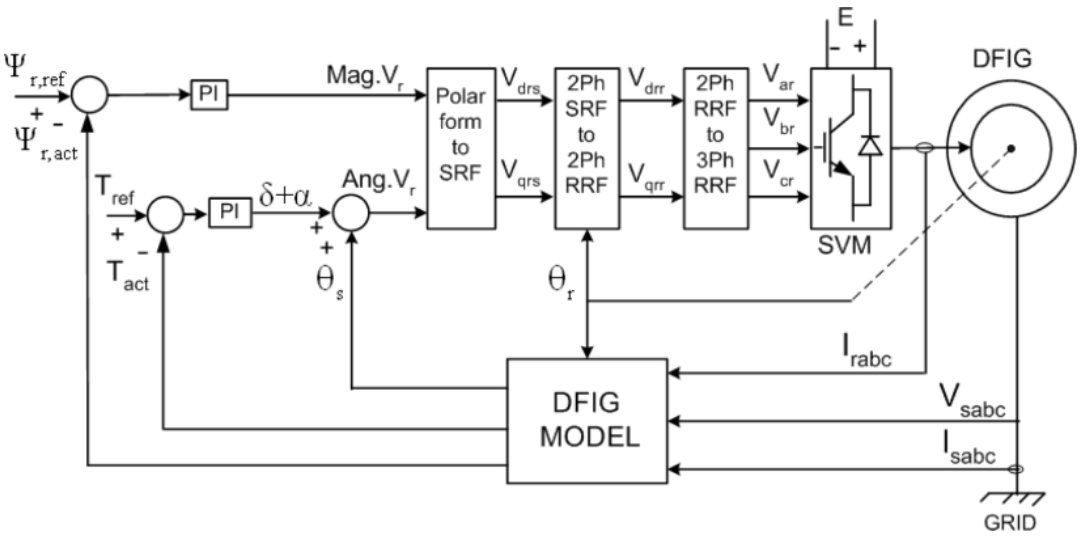

Figure 4.4: Direct torque control with SVM of a DFIM with trackside and position sensors [14]

1. The flux linkage hysteresis controller's state
2. The torque hysteresis controller's state
3. The estimated flux linkage angle, after being quantified into sectors

In short, the DFIM direct torque controller follows the following process:

1. Measure the rotor current, and the rotor voltage if it cannot be identified from the inverter state, using sensors.
2. Estimate the electromagnetic torque using Equation 4.2 and the magnetic flux using Equation 4.1.
3. A hysteresis controller compares the torque and flux with the reference, and outputs if they need to be increased, decreased, or kept the same.
4. The switching state is looked up from the switching table and immediately applied to the inverter.

When the state of a hysteresis controller changes, or when the estimated flux linkage orientation sector changes, the switching state of the voltage source inverter's switches is changed immediately. As a result, the switching frequency is not constant. This can sometimes be disadvantageous, because it makes it more complex to filter switching frequency components in a certain bandwidth. An advantage can be that the acoustic output of the motor becomes widebanded and therefore less noticeable.

Because of the deterministic logic, the direct torque controller has a much simpler implementation than a vector controller. This allows simpler control hardware to be used. However, the controller is also more difficult to tune. The main tuning parameters in a regular DTC controller are the speed controller parameters and hysteresis control bands. One way to make the controller more tunable is the use of a space vector modulator [14]. This will also reduce the torque ripple, but comes at the cost of some extra complexity. A schematic overview of this controller is shown in Figure 4.4. Note that this figure uses trackside and position sensors, which should preferably be replaced by estimators as described in Section 4.1.1 if used for the train application.

When the rotor velocity is close to synchronous velocity so that the induced voltage is low, an error in the estimated stator resistance may create a large relative offset in the estimated flux linkage vector, as can be seen in Equation 4.1. This stator resistance varies with temperature. With an erroneous flux linkage angle, the VSI switches may be applied wrongly, not stabilising the flux magnitude and torque anymore. The controller may therefore lose stability. This can partially be solved by determining the field orientation more robustly.

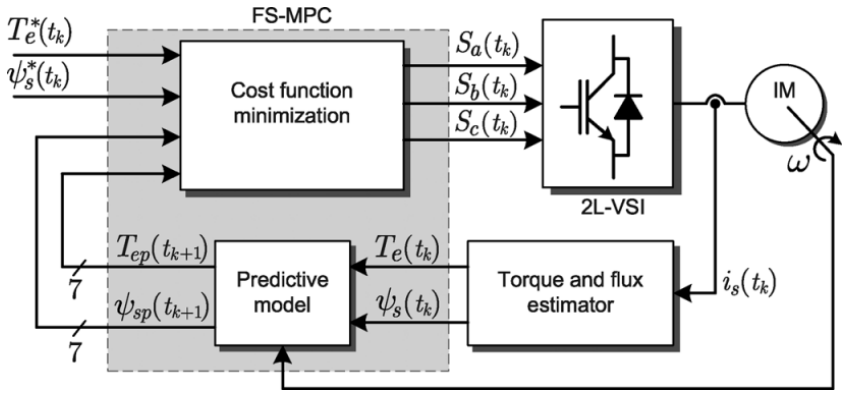

Figure 4.5: Generic model predictive machine controller structure [6]

The field orientation estimators as described in Section 4.1.1 can be used for a direct torque controller as well, however, this voids the main advantage of the controller which is the simplicity.

The current of the machine is controlled indirectly and is therefore not directly constrained. The current can be constrained in steady-state by limiting the torque and flux linkages. To constrain the current in transients as well, the references of the torque and flux have to be changed slowly by a predetermined ramp waveform [2].

4.3. Finite control set model predictive control

A model predictive controller (MPC) is a controller that uses a model to predict the future behaviour of the system and take appropriate action to steer it towards a reference. Given the model of the machine, an optimal solution can be calculated to steer the system towards the desired endstate [6]. However, such a calculation can be intensive to perform on an embedded processor, and are therefore incompatible with the multi-kilohertz control frequencies used in electric drives.

There is however a system property that can be exploited to speed up a MPC: a three-phase two-level voltage source inverter only has eight discrete voltage vectors that can be applied to the machine, as shown in Figure 4.3. This way, only a finite amount of scenarios have to be predicted to be able to find an optimal solution for the next control cycle. This is the basis of a finite control set model predictive controller (FCS-MPC) [6].

A model of the DFIM is essential to the MPC controller. Given the current state of the system, which form the initial conditions, a prediction can be done using the model for all possible inverter states. This outcomes of these scenarios are evaluated using a cost function, and the scenario with the best cost factor is applied to the inverter. A schematic of this process is shown in Figure 4.5. The amount of time between the current sample and the last predicted sample is the control horizon. The control horizon can be arbitrarily long, but it is often limited to one of two control cycles ahead since it becomes exponentially computationally intensive to predict more cycles ahead and is not beneficial for the control performance [6].

The complete process of a FCS-MPC is:

1. The relevant quantities are measured using sensors. These include the rotor current.
2. Using a model of the DFIM, the expected state of the DFIM after the next switching instant is calculated for all possible switching states. The expected state contains variables such as the rotor position, rotor current, electromagnetic torque, flux linkage, switching period and possibly more.
3. The expected states of the machine are compared to the reference. The difference, the error signal, is part of the cost function. Additionally, the expected outcomes are compared to the system constraints. If an outcome does not satisfy the constraint, additional terms are added to the cost function.
4. The cost function is weighted, resulting in a singular cost factor.

5. The switching state with the least associated cost factor is then applied to the converter.

A FCS-MPC compares to a direct torque controller in the sense that an optimal inverter state is chosen in each control cycle. However, instead of a rigid switching table based on two simple input parameters, a MPC is able to consider a lot of additional extra constraints or desires and can make a weighed decision between them. Additionally, rather than applying the selected switching state for the full control period, a variable active time followed by a dead time can also be used [3]. This can prevent over- and undershoot.

The weighting factors have a large influence on the behaviour of the controller. If a constraint has a relatively low weighing factor, it can be considered as a 'soft' constraint, which can be overridden if necessary. A weighting factor can even be time-invariant: For example, the current limit can be weighted by the current machine temperature, so that certain over-currents are allowed as long as the machine is cold. On the other hand, if the weighting factor is very large, it becomes a 'hard' constraint. However, optimising extra parameters may come at the cost of reducing the optimality of the main control objectives. A non-complete list of parameters which could be included in the cost function are [6]:

- The main control objectives: magnetic flux and electromagnetic torque.
- System constraints such as the rotor current.
- The amount of switching commutations. Possibilities include the spectrum shaping of the switching instants. For example, a frequency band can be selected for the inverter to operate in, or commutations resulting in certain frequency components can be penalised. This may be desirable to prevent interference with for example a radio system, and is an advantage over the relatively uncontrolled direct torque controller.
- Reducing the common-mode output voltage of the inverter.
- Balancing floating capacitor voltages of multilevel converters.

As a result, the model-predictive controller can be very flexible. Various works have been done which utilise this flexibility. One FCS-MPC controller adapted for use with a DFIM generator is explored in [11]. The controller there features an indirect matrix controller. The model predictive controller controls both DFIM power as well as the grid synchronisation and zero-current switching. This demonstrates the flexibility of a MPC controller with additional constraints. However, since the controller uses stator current sensors, it is unsuitable for immediate use with a shared-track system. Another MPC PQ-controller has been developed in [10] which uses a model of the DFIM magnetisation characteristics to be able to omit current sensors on the stator side, but it still uses stator voltage and position sensors.

The model used in the model predictive controller needs to be accurate for the predictions to match the reality, and thus to select a true optimal solution. Some inputs to the model are:

- The current inverter output state. This is a measure for the terminal voltage, which can be used to calculate the magnetic flux from.
- The rotor current. These can be measured directly by current sensors. Combined with the magnetic flux, this provides information about the electromagnetic torque.
- The rotor position. Like for the vector oriented controller, this can measured directly with a sensor or it can be estimated. For the train application, a sensored approach is not desired. Therefore, estimators are required. Section 4.1.1 lists possible estimator implementations.
- Additionally, the model may be made adaptive to various environment changes. For example, a temperature input may be included to make a better estimation of the winding resistance.

Method	Field-oriented control	Direct torque control	FCS-MPC
Controlled quantity	dq-currents	Torque and flux	Torque, flux, and others
Controller type	PI	Hysteresis	Predictive
Modulation	SVM-PWM	-	Optional spectrum shaping
Field orientation	Various	Induced voltage	Various
Machine model required?	Yes	No	Yes
Constraint handling	Current and voltage	Indirect	Any

Table 4.1: Summary of explored DFIM controller types

4.4. Comparison between explored controllers

A overview of the differences between controllers is listed in Table 4.1.

At the moment, embedded processors with advanced control capabilities become increasingly common. The controllers will be used in commercial grade vehicles, where the purchase price of a controller under 10 dollars will likely not be any issue whatsoever. The controller pricing probably will be even less of an issue by the time that this system, which is currently conceptualised, is going to be commissioned. For this reason, if other controllers have additional advantages, then these quickly outweigh the simplicity advantage of the direct torque controller. Therefore, the direct torque controller seems to be an unlikely candidate to use in the final train application. However, it is unclear at the moment how parameters such as the air-gap length change while cruising. It may be that a direct torque controller performs better with such a rapidly changing parameter, since the controller does not depend on a machine model.

It is clear that the model predictive controller excels in the handling of constraints and the simultaneous control of additional quantities. For this reason, the model predictive controller is preferred if for example the inverter for the DFIM would be designed as a multilevel converter, which requires active voltage balancing. In other cases, a field-oriented controller can also be a good candidate. Would it be beneficial for the shoreside power supply if the harmonics are concentrated in one frequency band? In that case, the field-oriented controller seems the clear choice.

Due to the aforementioned considerations, no final controller type choice is made in this thesis yet. However, this information can be used when a complete system is going to be designed.

5

Simulation on the application of the DFIM for the vactrain

In this chapter, simulations of a controlled doubly-fed induction machine will be described. Early concept testing is here performed using a relatively simple control algorithm: synchronous rectification of the rotor terminal voltage. This is equivalent to the emulation of a rotor resistor load. This allows the validation of the complete vehicle drive operational principle without adding complexity during this stage.

At first, the reasoning for choosing a simplified controller is given, as well as the implementation details. In the second section, the linear motor as designed in [1] will be simulated. The goal is to verify that the selected operation concepts combined with the designed linear machine function as intended. For the final vehicle, more advanced controllers may be used due to control limitations of the synchronous rectification principle. These limitations will be discussed in Chapter 7.

5.1. Controller type for simulation and testing

To test the operational principles of the system, a suitable controller had to be chosen. As described earlier in section 4.1.1, it is of large importance to synchronise the rotor voltage frequency with the slip frequency for the control of a DFIM. The described synchronisation could be performed using either using sensors or estimators. To be able to simulate and test the machines, such a controller could be implemented. However, the final choice of an advanced controller is dependent on unmade system design specifications. An advanced controller would also need elaborate development and tuning to reach its full potential. Therefore, to focus on the main scope of the thesis, a simplified controller has been used.

The core principle of the system is the usage of the DFIM as both propulsion and charging machine. This principle may instead be tested using a relatively simple controller. Choosing a simpler controller type allows to test the core operational principle more independently from the controller, allowing faster debugging. Therefore, the usage of a simple controller reduced the risk of delaying the report. For these reasons, two simple sensorless strategies were tested:

- **V/f control**
  A controler was used that applied a fixed and pre-determined voltage magnitude and frequency to the terminals of the rotor. In the laboratory setup, his frequency and voltage could be adjusted with the PC via the serial interface. The machine's speed could be adjusted by using the coupled DC machine.
- **Rotor resistance emulation**
  A very simple controller type was used were the applied terminal voltage was proportional to the measured current. This way, rotor resistors were emulated. This setup inherently synchronises the rotor

current frequency with the stator field frequency. Since the voltage is effectively rectified with a sinusoidal input current, this emulator can also be explained simply as a synchronous rectifier.

Both of these strategies have been tested in both simulation and laboratory settings, since it was preferred to use a controller type which could be confirmed to work in both settings. The processes and results of these tests are described in section 5.1.1 and section 5.1.2.

5.1.1. Strategy 1: V/f control

First, a V/f control strategy was tested in the laboratory in doubly fed mode. Here, an existing V/f controller implementation could be re-used which was used earlier to test the inverter in single-fed induction mode. The goal of the below-described test was to see whether this open loop V/f controlled rotor could be brought into synchronism with the stator field by rotating the rotor very close to the synchronous speed. This would be similar to the pull-in of a synchronous machine. If synchronism could be readily achieved, then this method was suitable to test the wireless charging concepts.

The V/f controller has been tested in laboratory setting first. The reason for this choice include:

- In a simulation, both the mechanical velocity of the machine and the stator voltage frequency can be set to an exact value. In contrast, the physical open-loop setup allows only approximate values, which makes the synchronisation more problematic in the laboratory setup compared to the simulation.
- The laboratory setup contains some (partly) unquantified properties. For example, the rotational inertia is not precicely known. Furthermore, the jaw coupling, which couples the DC machine to the DFIM, contains a small amount of slack. During synchronisation, a large torque ripple is anticipated, which may cause the slack in the coupling to bounce, which may affect the ability of the machine to synchronise.

Due to these reasons, a laboratory test has been performed first, as synchronisation this setup seems to be more difficult. In the case of problematic synchronisation, no further simulations needed to be performed, due to the desire of an equal controller type for the simulation and the laboratory setup.

It has been found that the rotor V/f controller was not able to get the DFIM into synchronous operation in the laboratory setup. The full process including the description of the setup has been described in section 6.2.1. For this reason, the rotor resistance emulator has been tested in simulation and in the laboratory setup as described in Section 5.1.2.

5.1.2. Strategy 2: Rotor resistance emulation

Doubly-fed induction machines have long been accelerated by connecting a variable resistor to the rotor terminals. By slowly ramping the resistance down during acceleration, the rotor current could be maintained at a nominal value with the full stator voltage and therefore magnetic field applied [7]. This allowed a gradual acceleration of a high inertia load without causing overcurrents. During this acceleration process, the rotor resistors absorbed power from the stator.

Since the use of rotor resistors is long-known and easy to conceptualise, a concept was laid out which is based on the emulation of a three-phase resistive rotor load R_{em}. This allows the manual control of the rotor current using the inverter. One major advantage is that no external sensors or estimators are required in order to control the angle of the applied rotor voltage. Instead, first, the existing current is measured using the inverter's two phase current sensors. Using the assumption that the common-mode current is zero, the current is then transformed to the alpha-beta reference frame. The voltage applied to the inverter terminals, and thus the rotor windings, is simply proportional to this measured current, as with a resistor:

$$V_{\alpha\beta} = I_{\alpha\beta} R_{em} \tag{5.1}$$

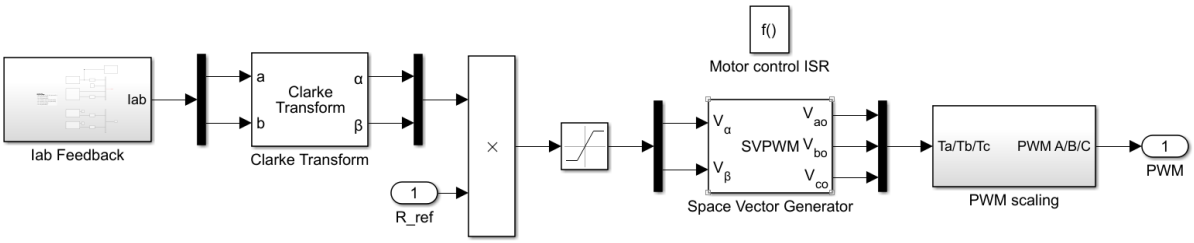

Figure 5.1: Laboratory implementation of rotor resistor emulation

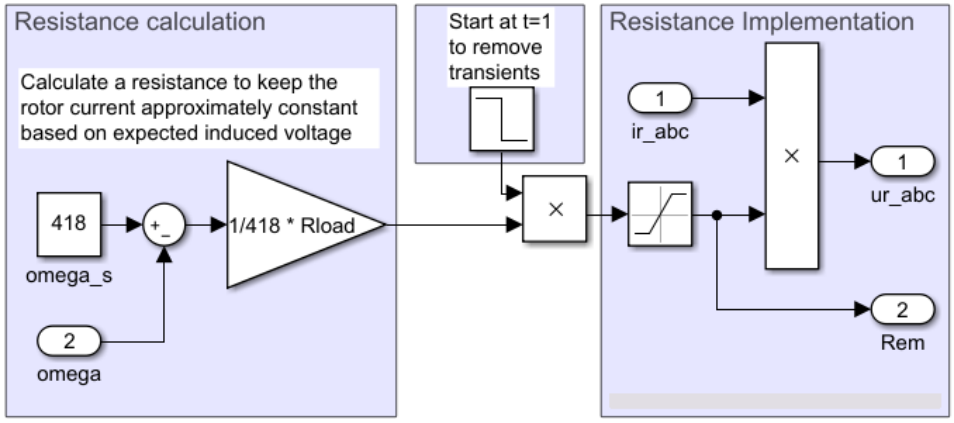

Figure 5.2: Calculation of the applied rotor resistance in simulation

This makes the voltage orientation equal to the current orientation, and a power factor of 1 is achieved. Figure 5.1 shows the Simulink model of this resistor emulation scheme used for the laboratory control setup.

In the simulation, the resistance is automatically adjusted to keep the rotor currents approximately constant. The magnetic flux linkage is also relatively constant, since the stator voltage is not changed. As a result, the electromagnetic torque is also constant, since this depends only on the rotor flux linkage and the rotor current as previously shown in Equation 3.9. The emulated resistance R_{em} is therefore kept proportional to the slip frequency, which is approximately equal to the rotor terminal voltage:

$$R_{em} = \frac{V_0}{I_0} \cdot \frac{\omega_0 - \omega}{\omega_0} \tag{5.2}$$

In this equation, V_0 and I_0 comprise the rated voltage and current with the rotor at standstill, and ω_0 and ω the synchronous and actual rotational speed. In the calculation of this resistance, the leakage inductances and machine winding resistances are not taken into account, nor are effects such as the skin effect. This causes the rotor current to be only approximately constant. Figure 5.2 shows the implementation of this resistance calculator in the simulation.

Early simulation and laboratory tests have shown that the rotor emulation concept can stably function as a means of electrically loading the DFIM. The process and results of the laboratory are further described in section 5.1.2. Since this emulator functions can function a means to test the concept of dually propelling and charging the vehicle, the rotor resistance emulator is chosen as the controller in the simulation and laboratory testing of the machine.

5.2. Synchronous rectification with the linear DFIM

In Chapter 6, lab tests of a synchronous rectifier on the rotary doubly-fed induction machine have been done. In this section, the functionality of this synchronous rectifier will be verified on the linear machine. Simula-

Parameter	Value	Unit
R_s	26.0	mΩ
R_r	86.2	mΩ
L_m	1.06	mH
$L_{\sigma s}$	286	µH
$L_{\sigma r}$	271	µH
Turns ratio	1.9542	-
Pole pitch	10	cm

Table 5.1: Stator-referred machine parameters of the linear DFIM [1]

Parameter	Value	Unit
R_S	26.0	mΩ
R_R	86.2	mΩ
L_M	221.1	µH
$L_{\sigma S}$	131.4	µH
$L_{\sigma R}$	0	µH

Table 5.2: Rotor-referred rotor flux oriented linear machine parameters

tions will be performed to confirm the total functionality, including charging at standstill and simultaneously charging and accelerating. For the simulation of the complete vehicle, the rotor-field based DFIM model has been used as developed in Chapter 3. The vehicle specifications as listed in Table 2.1 have been assumed. The electrical parameters have been retrieved from the linear machine as designed in [1] and are listed in Table 5.1. At the stator, a rotor-referred RMS phase voltage of 578V is applied with a frequency of 333 Hz. The rotor is loaded with a resistor of 1.508 Ohms at standstill. The rotor resistor is made to be proportional with the slip, so that is decreases to zero as the slip is decreases to zero. This will keep the rotor current approximately constant.

The power electronic converter is connected to the rotor side. Therefore, control calculations are done with rotor-referred quantities, so the stator quantities (R_s, L_m, and L_{ss}) need to be referred to the rotor side. To simplify the machine model, the rotor flux oriented model is used. First, the rotor leakage inductance is nullified by transforming to the rotor-oriented field model using the equation set as specified earlier in Equation 3.14. After this, the complete model is referred to the rotor side by using the turns ratio k_{tr} between stator and rotor:

$$X_s' = \frac{X_s}{k_{tr}^2} \tag{5.3}$$

The DFIM parameters are now all rotor-referred, but there are still two leakage inductances. A transformation is performed, as described in Section 3.5 where the rotor leakage inductance is eliminated while keeping the impedance as seen from the machine terminals equal. For this, the constant a as described there has been chosen as:

$$a = L - m/(L_m + L_{\sigma r}) \tag{5.4}$$

Equations 3.14 are used with this constant a to calculate the new rotor-referred rotor flux based model parameters. These parameters are listed in Table 5.2. These allow the use of a simulation model with only one leakage inductance.

In the simulation model, the resistance emulation block has been connected to the orange marked in- and outputs of the rotor circuit model, as shown in Figure 5.3. In the simulation, an average-value model is used: the effects of the pulse width modulation are not simulated. Since both the laboratory machine and the linear machine of the vehicle have significant inductances, and because the switching frequency of the MOSFET inverter is relatively high (20 kHz), the ripple currents will be low anyway and the average value model is

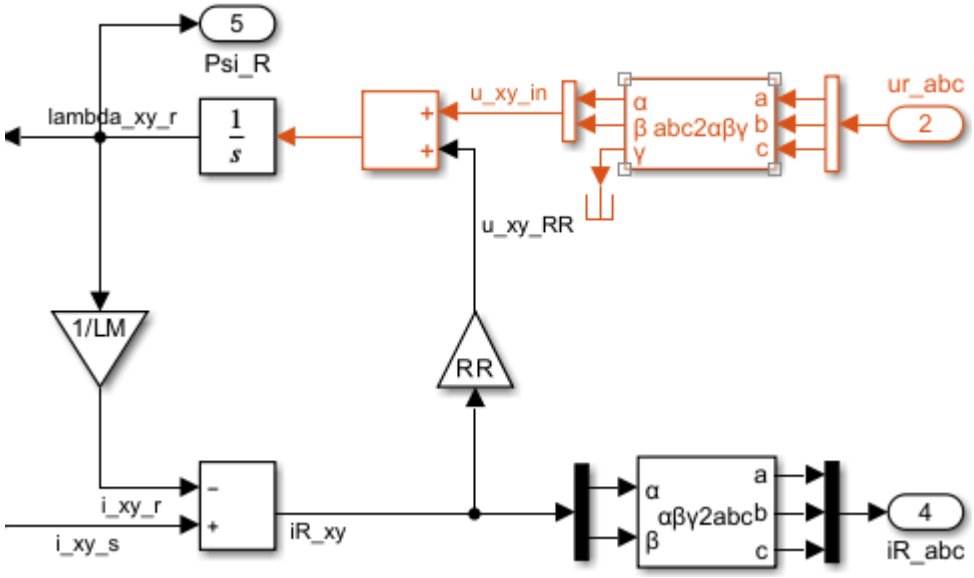

Figure 5.3: Simulation model of the DFIM rotor circuit

therefore a good approximation.

5.2.1. Synchronous rectification at standstill

During standstill, there is no mechanical power, so the only power flow across the air gap emerges as rotor power. From Figure 5.5c, it can be derived that the power transfer efficiency is 93,1%.

Figure 5.4 shows the voltage and current of both the stator and rotor during standstill. For clarity, only a single phase is shown. It can clearly be seen that the stator current lags the stator voltage by a significant amount. This materialises as a low power factor of 0.44, which can also be seen in Figure 5.5c. The rotor voltage lags the stator voltage as well, which is caused by the leakage inductance in the rotor circuit. This phase lag is not as large, since the large purely reactive magnetisation current is not included. The rotor current is perfectly in phase with the rotor terminal voltage, since it is loaded purely resistive.

5.2.2. Synchronous rectification during acceleration

A full acceleration profile of the vactrain vehicle has been simulated. An overview of the most important quantities is provided in Figure 5.5. It can be seen in subfigure (a) that the vehicle velocity approaches 200 km/h after 60 seconds, however, the traction force already gradually starts decreasing. This is caused by the simple resistance calculation, which does not consider the internal DFIM winding resistances nor the leakage inductances, and therefore overshoots the amount of applied resistance. In a final application, the traction force should be kept maximum, since it reduces the amount of (expensive) active track required. For that reason, the flux density and rotor current must be controlled more precisely.

With the rotor resistance emulator, only subsynchronous operation is possible, since the induced voltage and therefore the rotor current and torque reduce to zero as the machine approaches synchronous speed. The linear machine as designed in [1] has a nominal shore-side frequency f_s of 333 Hz and a pole pitch τ of 10 cm, making the synchronous velocity:

$$v_0 = f_s \cdot 2\tau = 333 \cdot 0.20 = 66.6 \text{ m/s} = 240 \text{ km/h} \tag{5.5}$$

For this reason, the simulated vehicle speed does not go above this maximum speed: As the speed increases towards it, the rotor current and the developed tractive force decrease significantly as can be seen in Figure 5.5.

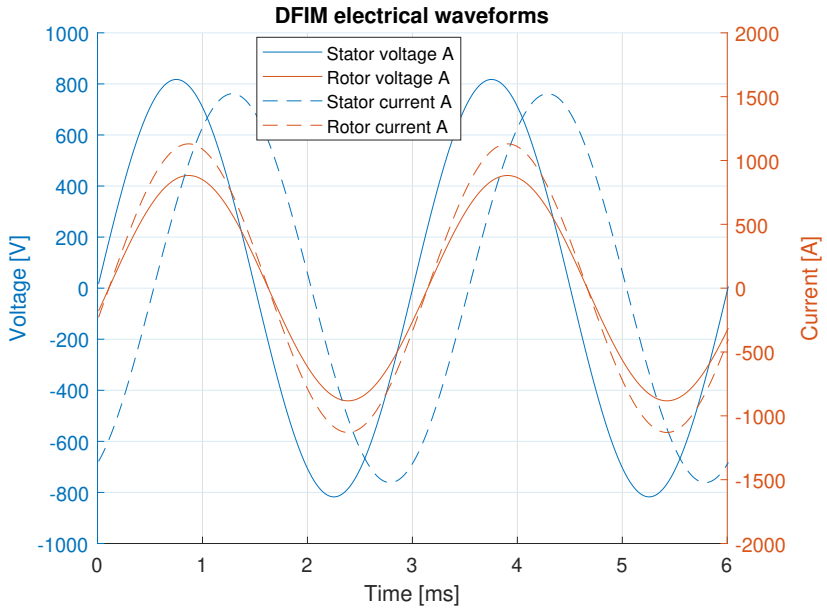

Figure 5.4: Simulated shore-side and vehicle-side DFIM currents

In the final application, the vehicle velocity is specified to reach 700 km/h, as listed earlier in Table 2.1. For this to achievable, either the synchronous velocity must be increased or the vehicle must be made to run supersynchronous. Alternatively, the pole pitch may be increased as well, but doing so would entail a complete redesign of the DFIM.

As described earlier in section 2.1.1, it is desired that the vehicle operates subsynchronously for most of the acceleration time, since this keeps the vehicle's battery from discharging. Therefore, raising the synchronous speed seems to be a far more realistic candidate than operating the vehicle supersynchronous. Although the DFIM as conceptualised in [18] and designed in [1] has a nominal shore-side frequency of 333 Hz, raising this frequency seems to be the most realistic candidate for final operation. However, if the maximum acceleration needs to be upheld, it will also be necessary to raise the maximum DFIM power. A solution could be to divide the track segments and operate the segments furthest from the station at a higher stator frequency. This will allow the vehicle to reach higher speeds without compromising the initial acceleration potential.

One additional consequence of increasing the synchronous velocity can be that the voltage drop across the leakage inductance becomes larger. This increases the need for a field controller, since the flux linkage becomes even more dependent on the loading current. In this thesis, the linear machine is only simulated using the original design parameters, so no simulation is performed yet with an adjusted shore-side frequency.

It can be seen in Figure 5.5d that the rotor flux linkage is not stable, but rather increases significantly as the vehicle reaches synchronous velocity. As the vehicle reaches synchronism, the rotor currents start to decrease. This reduces the voltage drop on the stator resistance and the stator leakage inductance of the DFIM, which increases the voltage across the magnetisation inductance. Using only a rotor resistance emulator, this flux linkage can not be stabilised, which is a major disadvantage over more advanced controller. Possible consequences and remediations of this issue are further discussed in section 7.1.2.

In Figure 5.5b, the simulated power share between the mechanical power and the rotor (vehicle battery) power is graphed. The quantities are shown relative to the stator power. It can be seen that the DFIM continuously operates with its maximum stator power, but the share of power delivered as mechanical power (P_m) increases linearly with the velocity v. This is expected, since the mechanical power with a constant acceleration is:

$$P_m = Fv = mav \tag{5.6}$$

With a maximum stator power of 1000 kW, a vehicle mass of 10 000 kg (Table 2.1), and a synchronous speed

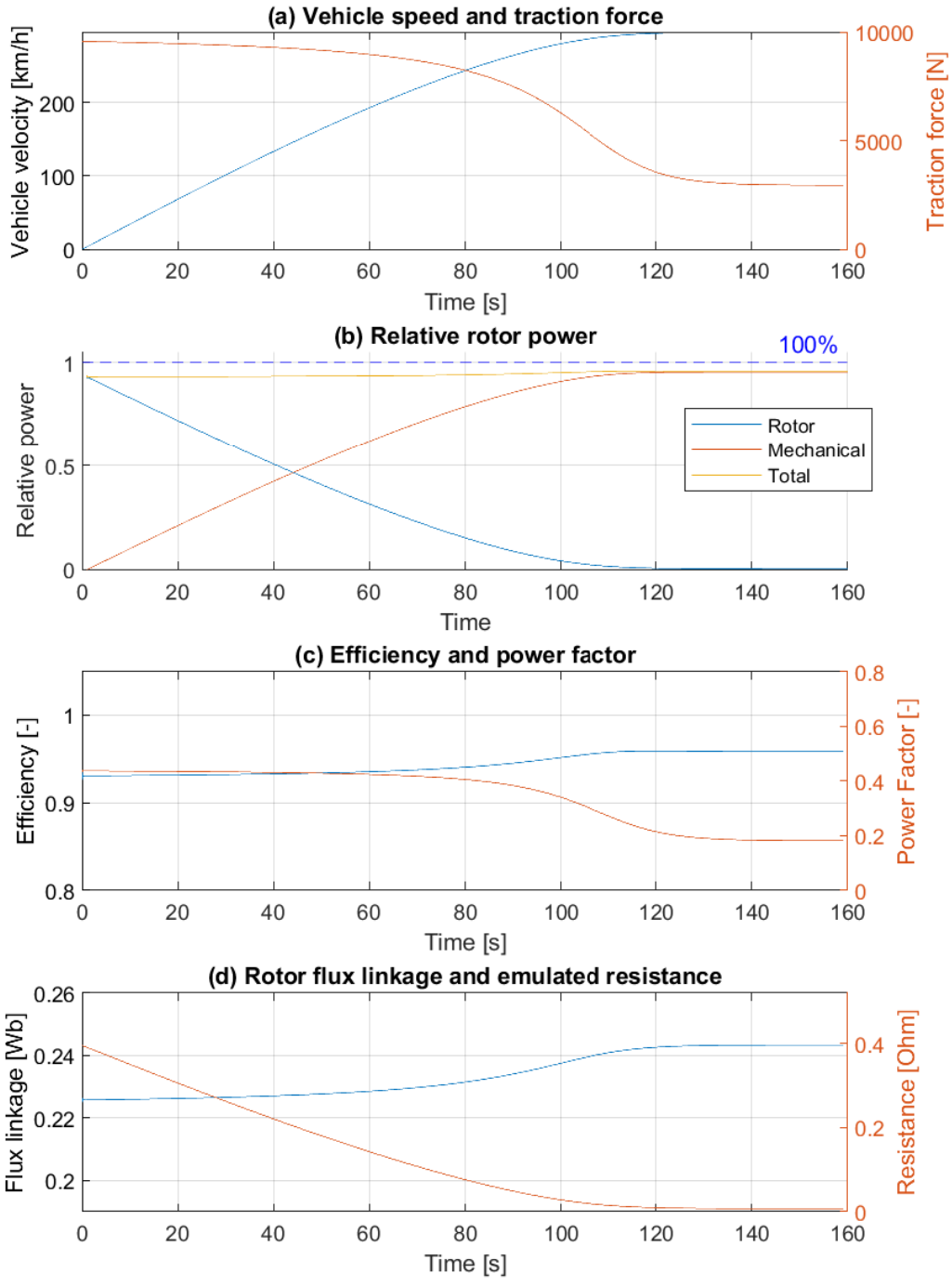

Figure 5.5: Simulation of the acceleration of the vactrain vehicle unit

of 240 km/h (Equation 5.5), a constant acceleration is expected of:

$$a = \frac{P_s^{\max}}{m v_0} = 1.5 \text{ m/s}^2 \tag{5.7}$$

This acceleration is comparable to a conventional subway train, and is therefore very reasonable for passenger comfort. The length of active track (l_{act}) to accelerate to 240 km/h (66.6 m/s) in time t becomes:

$$l_{act} = \frac{1}{2} a t^2 = \frac{1}{2} a \left(\frac{v_{max}}{a} \right)^2 = \frac{1}{2} \cdot \frac{v_{max}^2}{a} = 1.48 \text{ km} \tag{5.8}$$

An active track distance of 1.48 seems to be relatively short and therefore very economic, but it should be noted that it raises quadratically with the intended maximum speed, which is expected to be raised in a final product. With a maximum speed of 700 km/h and an equal acceleration, the minimum active track length becomes 12.6 km.

Since P_m is zero at standstill, when the vehicle velocity is zero, all stator power except for the losses should flow to the rotor and therefore vehicle battery. This shows clearly in Figure 5.5b. This confirms the applicability of using the DFIM as method for power transfer at standstill.

6

Laboratory verification of the operation principles

This chapter will describe the lab tests that have been performed to validate the system concept. The aim of the validation was to test whether efficient power transfer is indeed possible from the stator to the rotor, while providing propulsion at the same time.

In this thesis, the concept of simultaneous propulsion and wireless power transfer needed to be verified in a non-complex manner due to time constraints. For this reason, a simple control strategy was chosen, where no position sensor or electrical sensors on the stator side were required. Additionally, the laboratory tests done in this thesis focus on steady-state behaviour only.

6.1. Test setup

The machine under test is the rotary doubly-fed induction machine as listed in Table 3.1. Although the electrical parameters will be different compared to a final linear machine, the machines still share the same method of operation. Therefore, the conceptual tests can be done with this rotating machine, so that the development of a linear machine and the conceptual validation can be done simultaneously. In this section, the electrical and mechanical connections of the machine under test will be described. In Figure 6.1, a diagram of this lab setup is shown.

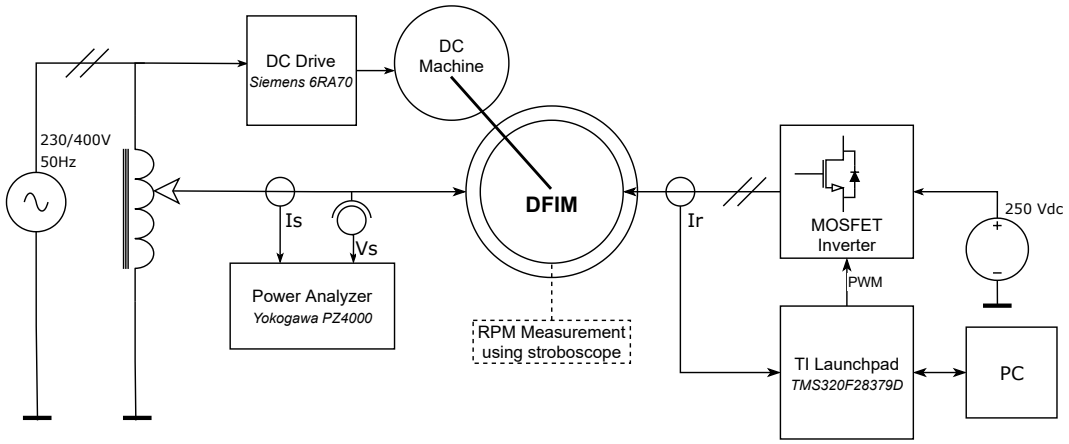

Figure 6.1: Diagram of the lab setup

MOSFET Inverter	
MOSFET Type	Cree C3M0120090J
MOSFET $R_{DS(on)}$	120 $m\Omega$
Control board	TI TMS320F28379D
DC Source	
Type	Delta SM 1500-CP-30
Voltage	250 V
Max. current	± 25 A
Power Analyser	
Type	Yokogawa PZ4000
Measurements done	Voltage, current, power factor, power

Table 6.1: Summary of the rotor interfacing hardware

6.1.1. DFIM Stator connection

The stator of the doubly-fed induction machine is connected to a variable three-phase autotransformer. This autotransformer is fed by the three-phase 400V phase-to-phase 50 Hz grid voltage. The stator could be shorted by turning the autotransformer's output voltage all the way down. A power analyser is inserted between the autotransformer and the machine's stator, to continuously monitor voltage, current, power factor and power.

6.1.2. DFIM Rotor connection

The rotor of the doubly-fed induction machine is available via a three-phase slipring. The three phases are then connected to a MOSFET inverter, containing a three-phase bridge. The power was supplied to the DC side by a bidirectional power supply, which was set to a voltage of 250V and a current limit of 25A. The inverter is controlled by a TI Launchpad TMS320F28379D development board. In all experiments, the switching frequency was set to 20 kHz. The Launchpad was also connected with a serial connection to the PC. The PC could program the Launchpad with the Matlab Simulink-software. Parameters could also be set through this serial connection. A screenshot of the PC interface is shown in Figure 6.2. The parameters of the rotor connection have been summed up in Table 6.1.

6.1.3. DC Machine

The doubly-fed induction machine is mechanically coupled to a DC machine. The DC machine was electrically driven by a *Siemens 6RA70* DC motor drive. The DC drive estimates the rotor speed by measuring the back-emf of the DC motor. A proportional control algorithm then tries to control the rotational speed by controlling the armature current. The combination of machine and drive could produce enough torque to control the speed of the DFIM under all conditions.

To enhance precision, the rotor speed was manually tuned for each measurement by adjusting the rotor speed control input until the rotor was synchronous with the output of a stroboscope.

6.2. Controller selection tests

The two controllers as described in Chapter 5 have been tested with the laboratory setup. The following sections will describe the testing processes.

6.2.1. Laboratory testing the V/f controller

The applied test consisted of the following steps:

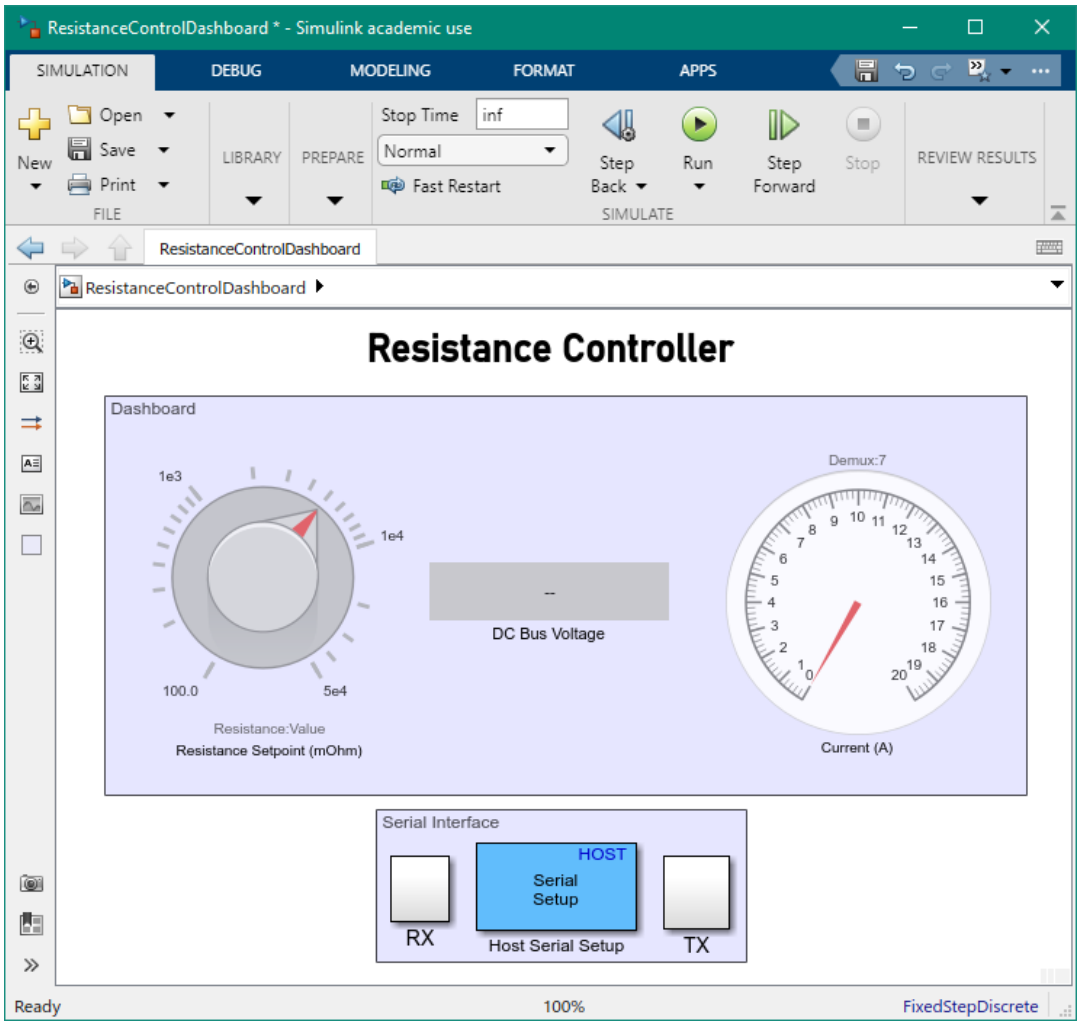

Figure 6.2: PC Interface for controlling the rotor resistance emulator

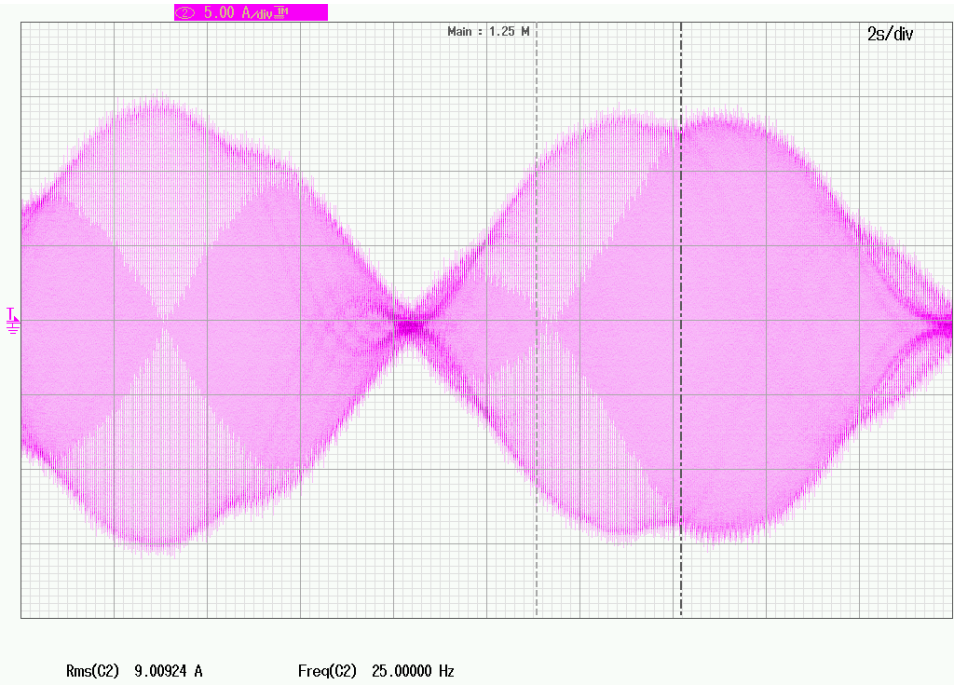

Figure 6.3: Rotor phase current waveform at near-synchronous stator and rotor fields

1. The machine's stator was connected to the grid via a variable autotransformer. Initially, the voltage was turned all the way down, as to short the stator.

2. A very low rotor voltage was applied by the inverter with a frequency of 25 Hz (half the nominal stator frequency).

3. The machine was turned by the DC machine at synchronous speed: 500 rpm. The speed control gain was set to a relative low value, in such way that the DFIM was able to vary the shaft speed ca. 1% with just 0.5 Nm of counteracting torque from the DC machine.

4. The rotor voltage magnitude was increased until the phase currents became 5 A. This magnetisation current has proven in earlier tests to be sufficient to provide torque to rotate the machine while keeping the current within the capabilities of the inverter. This torque was needed to hopefully pull the rotor and in synchronism with the stator field.

5. By increasing the voltage setting of the variable autotransformer, the 50Hz grid voltage was slowly be introduced to the stator. The stator voltage was not increased beyond 10V, as the current was already increasing to levels that were close to the current limits of the inverter.

6. The rotor current waveform was shown on an oscilloscope. If the 25 Hz current was modulated by a low frequency slip current, then it could be concluded that the rotor was not synchronous with the stator field.

Unfortunately, at ca. 10V stator phase voltage, the rotor current waveforms were showing no signs of synchronisation, while the current limits of the inverter and autotransformer came quickly in reach. A picture of this waveform can be seen in Figure 6.3. It can be seen that the 25Hz rotor voltage waveform was modulated by a very low difference frequency with a period of ca. 10 s. This means that the difference frequency was 0.1 Hz, or 0.4%. Unfortunately, even with this low difference frequency, there were no signs of 'pull-in' (synchronisation).

A reason why the rotor speed did not synchronise could be that the produced torque was too low, combined with the relative high rotor inertia. Because the the doubly-fed induction machine was mechanically coupled to the DC-machine with a steel jaw coupling, the complete rotor had a sizeable rotational inertia. With the

relative low current limit of the inverter, it may have been that the produced torque was simply too low to pull-in. Because the inverter current limit could not readily be increased, it was deemed to be prohibitively difficult to synchronise the rotor field with the stator field using this setup. Therefore, another testing strategy had to be found.

6.2.2. Laboratory testing the rotor resistance emulator

The rotor emulation system as described before in section 5.1.2 has been tested and has proven to function well. Figure 6.4 shows the current waveform of one AC phase as well as the DC bus current. It can be seen that the rotor current is nicely sinusoidal at large slip frequency. A 100 Hz component can be seen in the DC bus current, which may be due to a slightly unbalanced stator current. The relative harmonic content is a lot larger at low slip, which also causes a large DC current ripple.

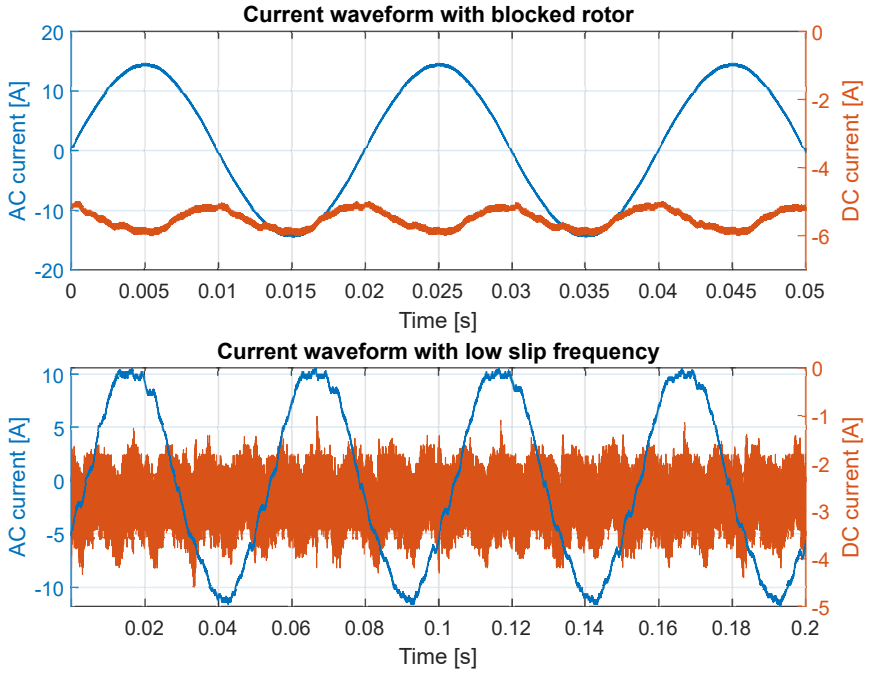

Figure 6.4: Measured rotor and DC currents

Although the current waveforms in Figure 6.4 can show a significant harmonic content and DC bus ripple current, it clearly shows that it is possible to regenerate power using this resistor emulation scheme. Therefore, this resistor emulation is used in this chapter to test the validity of the charging concept.

The major disadvantage of this emulation scheme is the lack of tuning possibilities. For example, the bandwidth of the output voltage is not limited, and noise of the current measurement will directly affect the applied terminal voltage. Furthermore, if the induced rotor voltage is not sinusoidal, in practice for example due to rotor slot effects, then the current will show these same harmonics. This reduces the power factor of the stator power supply.

6.3. Performance measurements

To keep the control system as simple as possible, R_{em} is only changed manually. The constant R_{em} is received from the serial interface, so that it can be changed from the PC. It is manually adjusted while viewing the rotor current waveforms on the oscilloscope, until this current got to the desired value. To keep the machine from changing speed, the speed of the doubly-fed induction machine was fixed by the DC machine.

RPM	I_r [A]	I_{dc} [A]	$\bar{I}_{ac}[A]$	P_{ac} [W]	Torque [Nm]
0	2.52	2.11	11.3	765	4.8
	5.06	4.24	11.9	1300	9.1
	7.50	6.26	12.8	1818	16.7
	10.00	8.18	14.0	2330	22.1
300	2.50	1.79	11.4	797	2.8
	5.00	3.34	12.1	1374	8.1
	7.50	4.82	13.1	1920	13.3
	10.00	6.15	14.5	2450	17.8
600	2.50	1.07	11.4	789	2.0
	5.00	1.96	12.2	1381	7.4
	7.50	2.74	13.2	1958	12.7
	10.00	3.50	14.6	2400	17.8
900	2.50	0.27	11.4	791	1.3
	5.00	0.45	12.4	1560	8.05
	7.50	0.56	13.9	2320	14.8
	10.00	0.53	15.1	2827	19.0

Table 6.2: Resistor emulation experimental results

With this setup, measurements were done at standstill, 300 RPM, 600 RPM and 900 RPM, so that all measurements were done under subsynchronous machine speeds. No supersynchronous speeds were tested because power flow would be opposite to the desired power flow: the inverter starts supplying power to the machine, which would discharge the battery in the final product. A three-phase phase voltage of 100 Vrms was applied to the stator. For all speeds, the rotor rms current was tuned to 2.5A, 5.0A, 7.5A and 10.0A. These currents represent an evenly spaced set within the thermal capabilities of the inverter. For every speed and current, the quantities DC current, AC stator current and power factor, and DC motor torque have been recorded. Here, the AC quantities are retrieved from the power analyser, and the DC machine torque from the DC machine drive status. The current flowing from the inverter is measured using a current probe connected to the an oscilloscope, which calculates the mean. This data is included in Table 3.3.

The efficiency of the complete charging setup is measured from AC power supply to the DC power supply. This way, all losses in the setup including machine, inverter and wire losses are included. The DC power is calculated using the 250V voltage setting of the power supply combined with the mean DC current:

$$P_r = V_{dc}\bar{I}_{dc} = 250\bar{I}_{dc} \tag{6.1}$$

It is required for the efficiency figure to know the power that could theoretically be transferred. This maximum power depends on the rotor velocity, as this affects the induced voltage in the rotor. If the losses due to the machine resistances are neglected, then the following equation holds: [5]

$$P_r \approx sP_s \tag{6.2}$$

The achieved efficiency can then be found by the ratio between the received power and the maximum achievable power:

$$\eta = \frac{V_{DC}\bar{i}_{DC}}{sP_s} \tag{6.3}$$

Furthermore, the rotor voltage is approximated to show some insights in the efficiency figures using the following equation:

$$V_r \approx \frac{P_{dc}}{3I_r} \tag{6.4}$$

These calculations are done for every measurement and are plotted in Figure 6.5.

As shown in Figure 6.5, the achieved efficiency is both dependent on rotor current and rotor velocity. In some conditions, the overall system efficiency is 85 to 90%. However, two effects occur which mainly affect this efficiency:

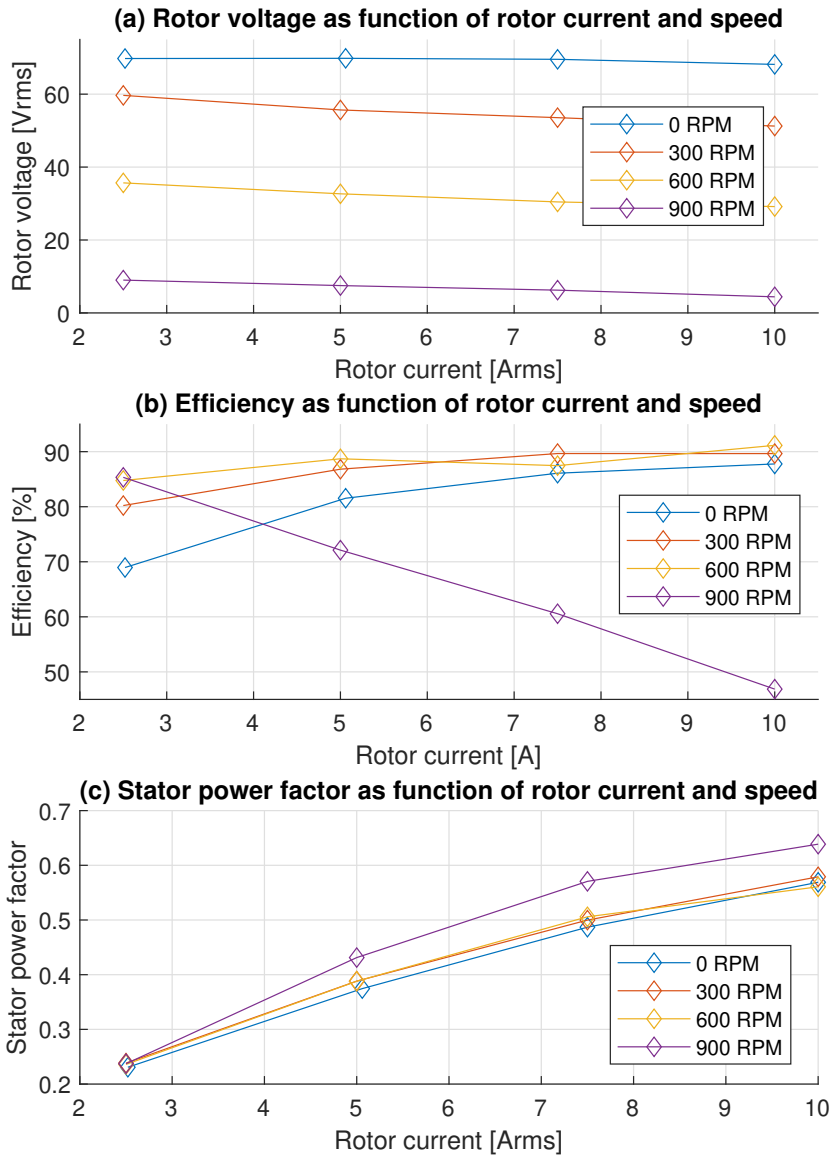

Figure 6.5: Efficiency figures of system validation test

Firstly, the machine draws a significant magnetisation stator current which is not transferred into the rotor inverter. This current will induce resistive and magnetic (eddy current and hysteresis) losses in the machine, which negatively affect the efficiency measurement. As the rotor current increases, the losses caused by this magnetisation current will not go up. Therefore, the fraction of power lost will become smaller, and the efficiency will generally go up with increased rotor current.

Secondly, as the rotor speed increases, the frequency of the magnetic field seen by the rotor becomes less, which reduces the induced voltage. In the final 900 RPM test, the induced voltage becomes very low (< 10 V). For this reason, any voltage drop caused by for example the stator or rotor resistance becomes very significant. This will therefore decrease the measured efficiency at high speed: while the absolute losses are comparable, the fraction of all losses of the total power is much higher at higher speed.

In some measurements, the power transferred to the rotor is only a fraction of the mechanical power, due to the relative speed of the rotor compared to the synchronous frequency. However, all losses are still included in the efficiency figure, including inverter losses. As these losses induced from mechanically powering the machine are also included in the losses, this makes the efficiency of the stator-to-rotor power transfer seem lower. Keeping this in mind, a power transfer efficiency of 85-90% is deemed to be very good.

6.4. Conclusions from laboratory tests

Lab tests have been performed where the possibility of vehicle charging using a doubly-fed induction machine is tested. A rotary machine has been used since it is readily available and represents the same method of operation. The efficiency of power transfer has been calculated at different rotor velocities.

Two control methodologies have been tested: A V/f control scheme and a rotor resistor emulation scheme. It was found that a V/f controlled rotor cannot be readily synchronised with the stator field under the test conditions. This shows that for a stable operation, the rotor current needs to be aligned with the stator field by the inverter, which may require either stator voltage and position sensors or a field estimator.

The second method tested, the rotor resistor emulation scheme, has shown to be able to stably transfer power from the stator to the rotor. Efficiencies as high as 91% have been recorded, but are highly dependent on the rotor current and rotor velocity. However, it shows that efficient power transfer while simultaneously providing propulsion is a definite and efficient possibility with this rotary doubly-fed induction machine.

A more advanced control scheme may be used to combat the limitations of the rotor emulation scheme. For example, a field oriented controller may be able to control the torque and speed more directly, while also improving the power factor. These limitations are further explored in Chapter 7.

7

Discussion

This chapter will describe the complications that were occurring while writing this thesis. First, the main limitations of the rotor resistance as means of controlling the doubly-fed induction machine will be discussed. Then, the results of the simulation of the vactrain concept will be discussed.

7.1. Limitations of rotor resistor emulation

In this thesis, the testing and simulation of the system concept was performed using the emulation of a rotor resistance. This was used as a simple control structure, which allows the use without information about for example the stator voltage and rotor position. However, during the development, some drawbacks could be identified. These drawbacks, and possible solutions, will be discussed in this section.

7.1.1. Transient response

The control structure is based on the steady-state model of the machine. In a steady-state phasor representation, a constant frequency operation is inherently assumed. Therefore, a steady-state model is not an accurate representation with for example sudden changes in load torque. The controller also is not equipped with a negative feedback loop. Unmodelled transients can therefore not be corrected.

7.1.2. Magnetic flux linkage control

In this rotor resistor emulated machine, the air-gap field strength is determined by the stator voltage and frequency, and the voltage drop across the stator resistance and leakage inductance. This voltage drop is strongly dependent on the load conditions. Therefore, with a fixed stator voltage and frequency and without rotor-side compensation mechanisms, the air-gap field strength cannot be held constant under different loading conditions. With a traditional rotary machine, the leakage inductance is often relatively small, which will make the air-gap field strength relatively independent on the load conditions. This makes open-loop V/f control suitable under some conditions. However, with the linear machine used in this thesis, the stator leakage is 27% of the magnetisation inductance. For this reason, the magnetisation becomes heavily dependent on the load conditions. An example of this is given in Figure 7.1.

For a more optimal control, the air-gap magnetic field strength should be maintained near the nominal value. This allows the full torque of the machine to always be developed, without causing magnetic saturation. Some solutions which aim to control the air-gap field strength better under all operating conditions are:

- Adjust the stator voltage based on the load conditions. This forces the stator to be supplied by a variable-voltage converter. Furthermore, a major disadvantage is that the stator voltage should only

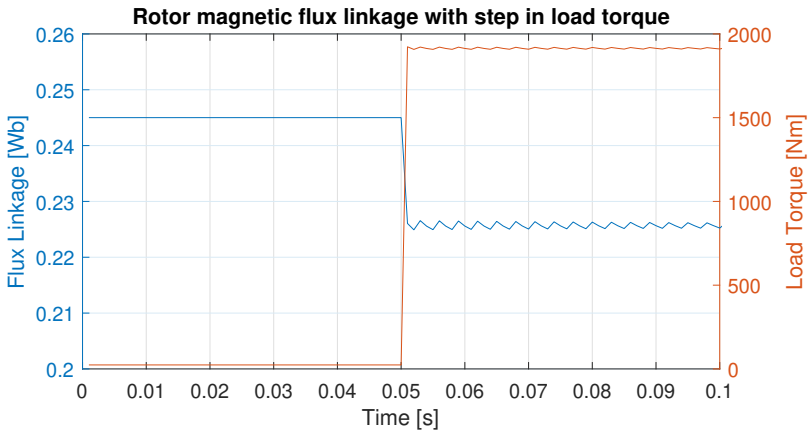

Figure 7.1: Change in machine flux linkage with an applied torque step

increase on the piece of track where the charging or accelerating vehicle is located, otherwise the magnetic field strength increases beyond nominal ratings where no vehicle is situated. This adds a lot of complexity to the system.

- Expand the existing control structure on the rotor side to cancel the voltage drop across the leakage inductance. This may be implemented by the emulation of a parallel load capacitor, of which the value is determined by a reverse machine model. However, this also means that the output voltage cannot be determined instantaneously anymore: the capacitor emulation adds a dynamic state. This increases the complexity of the control structure.
- Estimate the air-gap field strength, for example based on the induced voltage on the rotor side, and add a controller to keep this value constant. This may be done in several ways, for example with a field-oriented current controller or with a hysteresis control loop. This may be the more robust option. These two implementations will lead to either a field oriented control structure or a direct torque controller. Therefore, this steers the controller structure away from the simple resistor emulation.

It seems that this drawback of the resistor emulator cannot be overcome easily without adding complexity to the controller. Any added complexity nullifies the major advantage of this control scheme: its simplicity. For this reason, it is recommended to look into a more advanced controller, such as described in Chapter 4, in further research.

7.1.3. Lack of negative feedback

The lack of feedback poses some inherent limitations to the synchronous rectifier as machine controller. These include:

1. Since there is no closed-loop control, there can be imprecise reference tracking. For example, unmodelled effects or imprecise model parameters cause non-zero steady state errors. A closed-loop controller could eliminate this, for example using an error integrator.
2. The lack of a feedback loop prohibits possibilities to tune the controller. Without a way to filter frequency components, it is sensitive to noise and disturbance. A bandwidth limitation could help to prevent measurement noise on influencing the rotor voltage output.

7.2. Limitations of the vactrain simulation

Chapter 5 has described a system simulation where the complete vehicle is accelerated out of a station. However, this simulation has some known limitations:

1. Important parameters such as the vehicle's mass are based on estimations in [18]. However, these parameters can have a large influence on for example the acceleration time. This makes the simulation best interpreted only qualitatively, as a validation of the concept.
2. The simulation is done using a simple and idealised resistor emulator. A more advanced controller may be able to optimise the torque further, since it can be kept more constant with a closed loop controller.
3. The synchronous velocity of the stator is based on the design values from [1] which are mainly optimised for stationary charging. However, to be able to obtain larger speeds, the synchronous velocity must be raised as described in Section 5.2.2. The switch-over to this higher synchronous velocity is not simulated.

Due to these limitations, the simulation is not suited for quantitative analysis. However, it does confirm that the concept is functioning, which was its main goal.

8

Conclusion

The main research question of this thesis was:

How can a doubly-fed induction machine controller be designed to allow simultaneous propelling and charging a vactrain vehicle?

This research question is subdivided into multiple subquestions. In this chapter, these subquestions will be answered in the first sections. Thereafter, the lessons will be compiled into a final conclusion, listing the main findings of the thesis including recommendations.

8.1. Applicability of a DFIM for simultaneously charging and propulsion

The first research subquestion of this thesis was:

(a) To which extent is it possible to control the power flow to the batteries independent of the propulsion power?

The share of power supplied from the active track to the vehicle is a determined by the vehicle's velocity relative to the synchronous velocity, as is explained in Chapter 2 and Equation 2.2b. Furthermore, changing from acceleration to deceleration may cause unintended discharge of the batteries assuming unchanged vehicle and synchronous velocity. For this reason, it can be concluded that the power flow to the batteries cannot be controlled independently on the mechanical power of the machine.

The lack of independent control of power imposes a slight disadvantage to using the DFIM as power transfer method. However, it is not a insurmountable disadvantage. To prevent discharge of battery power during deceleration, the synchronous velocity of the shoreside power supply can be changed. In the simplest case, sections of track windings can be short circuited using trackside switchgear, which lets the DFIM operate in single-fed mode. This allows the vehicle to regenerate nearly all its kinetic energy during deceleration. At standstill, the vehicle can charge at full power if holding brakes are used.

There is some lost potential during regenerative braking: the battery may be able to absorb more power than regenerative braking provides, especially as the vehicle is nearly stopped. Using simple stator short-circuiting switchgear, there is no additional power transfer between shore and vehicle possible. This means that charging takes longer compared to a scenario where the battery was continuously charged at full power.

For the above-mentioned reasons, the power sharing characteristics must be taken into account during early system design. For efficient operations, the battery must be able to absorb the full deceleration power, as it cannot be transferred to the shoreside. Furthermore, brakes must be sufficiently strong to hold the vehicle at

standstill, for the vehicle to be able to charge. Braking force may be added using magnetic track brakes. It can be concluded that, although the charging power cannot be controlled independently, the system can still be designed to allow the nearly-full potential of dually using the DFIM.

8.2. Suitability of control algorithms

A major part of the thesis was determining a suitable controller. Therefore, a research questions of this thesis was:

(b) How can the machine be controlled to efficiently accelerate and decelerate the vehicle?

To answer this question in this thesis, multiple possible control methods have been reviewed. Of these, a simple resistance emulation scheme has been implemented on hardware. This section concludes the applicability of these control methods on the use of the DFIM in a railway application by answering the aforementioned research question based on the previous chapters.

8.2.1. Resistance emulation

A resistance emulator has been implemented in hardware for this thesis, and is tested with a rotary DFIM. This implemented resistance emulation system was successfully able to prove the real-world possibility of (in-motion) wireless charging using a DFIM, as well as providing tractive effort.

The simple structure of this controller leads to major limitations. For one, the control bandwidth is not controllable, which makes the current sensitive to external disturbances, which can cause unwanted losses or unexpected behaviour. Additionally, the controller cannot easily control the flux linkage of the machine. Finally, as the method is based around the steady-state model, it may not be able to control the machine as desired under transient conditions.

The aforementioned limitations are inherent of the controller. Therefore, while this control setup has been able to prove the applicability of the DFIM for the vactrain application, the controller will not be ideal for a final, automated application. For this reason, section 8.2.2 will describe which of the explored other types of controllers will likely function better in a final application, answering the research question.

8.2.2. Best suited controller types

A review of possible, more advanced, controller candidates has been provided in Chapter 4. This review will be used to summarise the main findings of the two research questions regarding the controller type.

(c) Which type of controller is suitable for combining simultaneous propelling and charging the machine?

Three different candidates have been given: field-oriented control, direct torque control, and model predictive control. The power transfer from stator to rotor is inherent with a DFIM: if a torque is delivered, and there is a non-zero slip, then power will be transferred. All mentioned controllers are able to control the torque and thereby automatically the power flow to the battery as well.

The best suited controller is dependent on the final design criteria. At the moment of writing this thesis, it is not known how the exact track-side and vehicle hardware will look. For this reason, the best suited controller types are summarised below with their major advantages. A choice can be made later in the system design process based on the requirements.

- If it is most important that the inverter switching frequency spectrum is very narrow-banded, and that the current ripples are as small as possible, then field-oriented control is the preferred candidate, since SVM-PWM controllers use a constant switching frequency.
- If it is most important to keep the controller as simple as possible, a direct torque controller is preferred.

Direct torque controllers are able to directly function under all conditions (active track, with possibly changing stator frequency, and passive track) without requiring modifications. No information about stator quantities is required.

- If it is most important to have a flexible controller that can accommodate simultaneous constraint handling, then a model predictive controller is the best candidate. A model predictive controller can for example balance the capacitor voltages in a multi-level inverter with only a very simple addition in the cost function.

(d) How is it possible to omit a position sensor to effectively control the DFIM?

In every DFIM controller, it has been essential to keep the rotor field angle synchronous to the field angle. If the voltage applied to the rotor has a slightly different frequency compared to the slip frequency, than the rotor current will be modulated by the difference frequency, causing serious torque fluctuations. Therefore, the applied rotor voltage must have exactly the slip frequency, and indirect field estimators are ruled out.

Since the rotor's position is not fixed, it seems essential to have knowledge about the position as well as the stator field angle. However, it would add complexity to include position sensors and to communicate the state of the stator field to the vehicle. For this reason, a field estimator is suggested.

In a direct torque controller, the magnetic field strength and angle are estimated continuously from the induced voltage, as explained in Equation 4.1. Such a calculation can also be used for field-oriented controller types. To keep the induced voltage intact, and therefore the measured field angle reliable, the slip frequency must not become zero. For this reason, a trackside synchronous velocity well above the maximum achievable vehicle velocity is advised.

If a field-oriented controller is used, a PLL method is advised, since the synchronous velocity speed can then be lowered to the maximum speed of the vehicle. A decrease of stator frequency increases the power factor, and therefore efficiency.

Finally, if a model predictive controller is chosen, a high-frequency voltage injector can be used for the controller. This allows the vehicle to reach synchronous velocity under active track operation, but it requires extra trackside hardware and a separate estimator must be used when operating on passive track.

8.3. Final conclusion

The main research question of this thesis was:

How can a doubly-fed induction machine controller be designed to allow simultaneous propelling and charging a vactrain vehicle?

A common field-oriented controller, direct torque controller, or model predictive controller can all be used to control a vactrain vehicle. The final choice depends on system design requirements. Controllers which use track-side sensors are undesired. Therefore, some controllers require estimators to be able to eliminate sensors.

The difficulties which were directly related to the railway application of a DFIM have been paired with a possible solution. As part of answering the main research question, and for future reference, these have been summarised below in Table 8.1.

It can be concluded that a doubly-fed induction machine has been successfully used to transfer power as well as propel a rotor in a lab setting. Additionally, simulations have shown that the same principle applies with a linear machine design. The achieved efficiency was 91% (maximum) in the low-power lab setting and 93% in the high-power simulation.

Hurdle	**Suggested solution**
Rotor power dependent on vehicle velocity and tractive force	Take the expected power share into account during early system design (especially of the battery system). Use magnetic track brakes to hold the vehicle during standstill charging.
Rotor frequency must be exactly synchronised to slip frequency	Use the induced voltage in rotor for field estimation, also eliminating the need for position sensoring. Additionally, this can allow seamlessly transitioning to shorted stator use. Alternatively, modulate a high-frequency signal on the stator voltage.
Battery drains while regenerative braking during subsynchronous operation	Include stator-winding short circuit switches in the active track section, to make the DFIM slip negative.
DFIM is designed for a 240 km/h synchronous velocity, while the target velocity is 700 km/h	Increase the stator frequency at sectors a certain distance away from the station. This allows for a high initial acceleration without having to increase DFIM design power, and without having to spend energy from the vehicle side.

Table 8.1: Suggested solutions to encountered hurdles

Bibliography

[1] Belkassem Becetti. Design and optimization of linear doubly-fed induction machine for wireless charging operation of novel vactrain system. Master's thesis, TU Delft Electrical Engineering, Mathematics and Computer Science; TU Delft DC systems, Energy conversion & Storage, July 2021. URL http://resolver.tudelft.nl/uuid:06294eb1-fdc2-4769-affd-6c8403d4524f.

[2] D. Casadei, F. Profumo, G. Serra, and A. Tani. FOC and DTC: two viable schemes for induction motors torque control. *IEEE Transactions on Power Electronics*, 17(5):779–787, sep 2002. doi: 10.1109/tpel.2002.802183.

[3] S. Alireza Davari, Davood Arab Khaburi, and Ralph Kennel. An improved FCS–MPC algorithm for an induction motor with an imposed optimized weighting factor. *IEEE Transactions on Power Electronics*, 27(3):1540–1551, mar 2012. doi: 10.1109/tpel.2011.2162343.

[4] Rik De Doncker, Duco Pulle, and André Veltman. *Advanced Electrical Drives: Analysis, Modeling, Control*, volume 52. January 2011. ISBN 9789400701793. doi: 10.1007/978-94-007-0181-6.

[5] Lianwei Jiao, Boon-Teck Ooi, Géza Joós, and Fengquan Zhou. Doubly-fed induction generator (DFIG) as a hybrid of asynchronous and synchronous machines. *Electric Power Systems Research*, 76(1):33–37, September 2005. ISSN 0378-7796. doi: 10.1016/j.epsr.2005.04.007. URL http://www.sciencedirect.com/science/article/pii/S0378779605001422.

[6] S. Kouro, P. Cortes, R. Vargas, U. Ammann, and J. Rodriguez. Model predictive control—a simple and powerful method to control power converters. *IEEE Transactions on Industrial Electronics*, 56(6):1826–1838, jun 2009. doi: 10.1109/tie.2008.2008349.

[7] C.S. Moo, C.C. Wei, C.L. Huang, and C.S. Chen. Starting control of wound-rotor induction motors by using chopper-controlled resistance in rotor circuit. In *Conference Record of the IEEE Industry Applications Society Annual Meeting*. IEEE. doi: 10.1109/ias.1989.96962.

[8] S. Muller, M. Deicke, and R. W. De Doncker. Doubly fed induction generator systems for wind turbines. *IEEE Industry Applications Magazine*, 8(3):26–33, May 2002. ISSN 1558-0598. doi: 10.1109/2943.999610.

[9] C. Nagamani, G. S. Ilango, M. A. Asha Rani, and A. Prasanthini. Computation of rotor position of DFIM using Rotor side Phase Locked Loop. In *2016 National Power Systems Conference (NPSC)*, pages 1–6, December 2016. doi: 10.1109/NPSC.2016.7858861.

[10] Shafiq Odhano, Sandro Rubino, Mi Tang, Pericle Zanchetta, and Radu Bojoi. Stator Current-Sensorless-Modulated Model Predictive Direct Power Control of a DFIM With Magnetizing Characteristic Identification. *IEEE Journal of Emerging and Selected Topics in Power Electronics*, 9(3):2797–2806, June 2021. ISSN 2168-6785. doi: 10.1109/JESTPE.2020.3024679.

[11] Alejandro Olloqui, José L. Elizondo, Marco Rivera, Manuel E. Macías, Osvaldo M. Micheloud, Rubén Peña, and Patrick Wheeler. Model-Based Predictive Rotor Current Control Strategy for Indirect Power Control of a DFIM Driven by an Indirect Matrix Converter. *IEEE Transactions on Energy Conversion*, 36 (2):1510–1516, June 2021. ISSN 1558-0059. doi: 10.1109/TEC.2020.3038471.

[12] N. El Ouanjli, A. Derouich, A. Chebabhi, and M. Taoussi. A comparative study between FOC and DTC control of the Doubly Fed Induction Motor (DFIM). In *2017 International Conference on Electrical and Information Technologies (ICEIT)*, pages 1–6, November 2017. doi: 10.1109/EITech.2017.8255302.

[13] Ryszard Palka and Konrad Woronowicz. Linear Induction Motors in Transportation Systems. *Energies*, 14(9):2549, January 2021. doi: 10.3390/en14092549. URL https://www.mdpi.com/1996-1073/14/9/2549.

[14] B. B. Pimple, V. Y. Vekhande, and B. G. Fernandes. New direct torque control of DFIG under balanced and unbalanced grid voltage. In *TENCON 2010 - 2010 IEEE Region 10 Conference*, pages 2154–2158, November 2010. doi: 10.1109/TENCON.2010.5686748. ISSN: 2159-3450.

[15] D. D. Reigosa, F. Briz, C. Blanco, and J. M. Guerrero. Sensorless Control of Doubly Fed Induction Generators Based on Stator High-Frequency Signal Injection. *IEEE Transactions on Industry Applications*, 50 (5):3382–3391, September 2014. ISSN 1939-9367. doi: 10.1109/TIA.2014.2303255.

[16] Shuying Yang, Xing Zhang, Chongwei Zhang, Zhen Xie, and Shengcong Chai. Study on vector control for double-fed induction machine with stator windings short circuited. In *2010 International Conference on Computer, Mechatronics, Control and Electronic Engineering*, volume 3, pages 519–522, August 2010. doi: 10.1109/CMCE.2010.5610268. ISSN: 2159-6034.

[17] Tetsuo Uzuka. Faster than a speeding bullet: An overview of japanese high-speed rail technology and electrification. *IEEE Electrification Magazine*, 1(1):11–20, sep 2013. doi: 10.1109/mele.2013.2271839.

[18] Andre Veltman, Paul van der Hulst, Marco Jonker, and Henk Polinder. Tunnel-vision on economic linear propulsion? In *2019 12th International Symposium on Linear Drives for Industry Applications (LDIA)*. IEEE, jul 2019. doi: 10.1109/ldia.2019.8771014.

[19] Longya Xu and Wei Cheng. Torque and reactive power control of a doubly fed induction machine by position sensorless scheme. *IEEE Transactions on Industry Applications*, 31(3):636–642, May 1995. ISSN 1939-9367. doi: 10.1109/28.382126.